Effects of airmass type on the interaction between warm stratocumulus and underlying cumulus clouds in the marine boundary-layer

By G. M. MARTIN[1]*, D. W. JOHNSON[1], P. R. JONAS[2], D. P. ROGERS[3], I. M. BROOKS[3] and R. W. BARLOW[1]

[1] *Meteorological Office, UK*
[2] *UMIST, UK*
[3] *Scripps Institution of Oceanography, USA*

SUMMARY

Decoupling of the marine boundary-layer beneath stratocumulus clouds and the formation of cumulus clouds at the top of a surface-based mixed layer (SML) have frequently been observed and modelled. Observations of the cumulus–stratocumulus interaction during a Lagrangian study as part of the Atlantic Stratocumulus Transition Experiment (ASTEX), detailed in Martin *et al.* (1995), were made in an airmass which, although it was over the sea, was highly polluted, since it had recently come from industrial Europe. These observations suggested that the interaction was associated with significant changes in the stratocumulus thickness, microphysics and radiative properties. However, it was suggested that such changes may vary according to the type of airmass in which the cumulus–stratocumulus interaction was taking place. In this paper, two further case studies of the interaction in airmasses from different locations, exhibiting different thermodynamic properties and different levels of pollution, but being generally cleaner than that in the ASTEX Lagrangian study, are analysed to try to assess the influence of airmass type on the interaction. Although the cloud liquid-water content in the stratocumulus generally increases locally in a region of cumulus cloud penetration, the changes in the droplet spectrum which result from mixing between the cumulus and stratocumulus droplets depend on the individual droplet spectra in the two cloud types. This, in turn, is influenced by the aerosol characteristics in the boundary layer, the updraught velocities associated particularly with the cumulus clouds, and the actual and relative cloud thickness of the cumulus and stratocumulus. The effects of penetrating cumulus clouds on the droplet-effective-radius in the stratocumulus, and hence on the cloud radiative properties, may therefore differ significantly between boundary layers in which the interaction is occurring.

KEYWORDS: Airmass Cumulus Decoupling Marine boundary-layer Stratocumulus

1. INTRODUCTION

A common observation in cloud-topped marine boundary-layers is the presence of cumulus clouds below the stratocumulus, some of which are penetrating the overlying cloud layer (James 1959; Nicholls 1984; Slingo *et al.* 1982; Martin *et al.* 1995; Miller and Albrecht 1995; Wang and Lenschow 1995). This situation occurs frequently around the British Isles (Nicholls 1984), and was observed on seven out of ten research days during the First ISCCP (International Satellite Cloud Climatology Project) Regional Experiment (FIRE) off the coast of California in the summer of 1987 (Paluch and Lenschow 1991). During the Atlantic Stratocumulus Transition experiment (ASTEX), which took place in the Azores during June 1992, cumulus rising into stratocumulus was the most frequently observed cloud type (Albrecht *et al.* 1995), and it was suggested (Bretherton 1992) that the occurrence of cumulus–stratocumulus interaction may be inherent in the transition from stratocumulus to trade-wind cumulus in the subtropics.

The existence of cumulus clouds beneath a stratocumulus layer is an indication that the boundary layer is not well-mixed down to the surface, and that a slightly stable transition layer has formed between the upper layer (comprising the cloud and sub-cloud layers) which is driven by cloud-top cooling, and the lower layer which is driven by surface fluxes (the surface-based mixed layer, SML), as reported by Nicholls (1984), Albrecht *et al.* (1985), Nicholls and Leighton (1986), Turton and Nicholls (1987), Albrecht *et al.* (1988), Paluch and Lenschow (1991) and Hanson (1991). The stable region can occur as a result of shortwave heating within the cloud layer (Slingo *et al.* 1982; Nicholls 1984; Rogers and

---

Koračin 1992), in which case it often exhibits a marked diurnal cycle (Bougeault 1985), or from evaporation of drizzle beneath the stratocumulus-cloud base (Albrecht 1989; Nicholls 1984). Both of these effects have a stabilizing influence on mixing throughout the boundary layer, impeding the transfer of turbulent kinetic energy (TKE) between the cloud top and the surface. As the humidity of the SML builds up during the day, cumulus clouds may form if the SML becomes conditionally unstable, some of which may grow up into the overlying stratocumulus. It has been suggested (Nicholls 1984; Martin *et al.* 1995) that such clouds could act to link the cloud layer and SML. The local enhancement of the moisture flux could counteract the effects of entrainment of warmer, dry air from above the temperature inversion into the cloud, which may otherwise result in thinning of the stratocumulus layer.

Observations of the boundary layer and cloud microphysical characteristics associated with cumulus–stratocumulus interaction during a 34-hour Lagrangian study as part of ASTEX were detailed in Martin *et al.* (1995). These observations suggested that the interaction was associated with significant changes in the stratocumulus thickness, microphysics and radiative properties. It was also suggested that such changes may vary according to the type of airmass in which the cumulus–stratocumulus interaction was taking place, that is, whether the airmass has recently passed over a land area and can therefore be termed a 'continental' airmass, in which case there may be high concentrations ($\sim$1000 cm^{-3}) of anthropogenic aerosol in the boundary layer, or whether the airmass has spent considerable time over the sea and can therefore be termed a 'maritime' airmass, in which case the aerosol concentrations in the boundary layer may be small ($\sim$10–100 cm^{-3}) and composed of natural particles such as sea salt or ammonium sulphate (see Martin *et al.* 1994). In this paper, we use three case studies of the interaction (including that described in Martin *et al.* 1995), in airmasses from different locations, exhibiting different thermodynamic properties and different levels of pollution, to try to assess this variation. These are described individually in section 3, and the similarities and differences between them are discussed in section 4.

2. INSTRUMENT DESCRIPTION

Most of the measurements detailed in this paper were made from the Hercules C-130 aircraft of the Meteorological Research Flight (MRF) (some measurements made by the National Center for Atmospheric Research (NCAR) *Electra* aircraft during the ASTEX Lagrangian study have been taken from Martin *et al.* (1995) for use in sections 3(a) and (4). The C-130 is an instrumented atmospheric-research aircraft which is equipped to measure the radiative and microphysical properties of stratocumulus and cumulus clouds. Flight patterns consist of slow ascents or descents (at 2.5 m s^{-1} in the boundary layer and 5 m s^{-1} in the free troposphere) and vertical stacks made up of several 10-minute straight and level runs at 100 m s^{-1}, at different altitudes. Details of much of the instrumentation and its performance are given in Rogers *et al.* (1995). The instruments used to obtain the microphysical data analysed here were a Particle Measuring Systems (PMS) Passive Cavity Aerosol Spectrometer Probe (PCASP) which measures aerosol particles in the range 0.1 to 3.0 μm diameter, a PMS Forward Scattering Spectrometer Probe (FSSP), which can measure droplets in the range 0.5 to 47.0 μm diameter, and a PMS 2D cloud probe (2DC) which measures droplets in the size range 25 to 800 μm diameter (Baumgardner 1989). A thermal-gradient diffusion chamber (Saxena and Kassener 1970) was used to measure Cloud Condensation Nucleus (CCN) activity spectra. The output from the FSSP and PCASP is in the form of size spectra, from which bulk quantities such as droplet or particle effective radius, liquid-water or aerosol mass content, and droplet or particle

concentration can be calculated. The 2DC probe produces images of individual water droplets, and these can also be processed to give size spectra from which the above bulk parameters can be derived.

Regular maintenance and calibration of the PMS probes are carried out in order to minimize the potential measurement errors associated with these instruments. Standard corrections such as the calculation of the effective beam diameter and the activity correction (Baumgardner 1983) are applied to the FSSP concentration measurements. Baumgardner (1983) presents an analysis of the estimated accuracy in the measured FSSP concentrations when these corrections are applied (17%) compared with the accuracy when they are not applied (45–100%). Sizing errors in the FSSP are kept to a minimum by regular calibrations using glass microspheres. However, uncertainties are thought to be introduced by laser inhomogeneity (Baumgardner and Spowart 1990), coincidence of droplets in the beam (Cooper 1988) and the limited response time of the probe's electronics (Baumgardner and Spowart 1990). Such errors are estimated (Baumgardner 1983) to result in an average sizing uncertainty of 17%. The PCASP is calibrated regularly using latex nanospheres; accuracy in PCASP concentrations is achieved by continuously measuring the flow rate through the sample volume and applying an activity correction similar to that used for the FSSP. Although PCASP measurements can be made in water cloud, such measurements are often very noisy, with spurious high concentrations and large particle sizes. It has been suggested (J. Hallett, personal communication) that this may be the result of droplet shattering on the probe tip, which will be more effective as the diameter of the droplets and the speed of the aircraft increase. Since it is not possible to remove such effects from the data, only PCASP measurements made when out-of-cloud are used in this study. The CCN counter requires discrete air samples to be collected in an alleviator, where a neoprene bladder is used to pressurize the sample to cabin pressure. The alleviator is large enough for several samples to be extracted from it so that CCN supersaturation spectra can be determined. Unfortunately, this technique is very slow, so that only one CCN supersaturation spectrum can be obtained during a typical horizontal run. The CCN counter is calibrated by photographing and counting the activated droplets within a known volume of the laser beam and comparing this concentration with the peak voltage from the scattering photodetector.

3. CASE STUDIES OF CUMULUS–STRATOCUMULUS INTERACTION

(a) Lagrangian study, 19–20 June 1992

This series of experiments, which took place in the vicinity of the Azores, was described in some detail in Martin et al. (1995), and many of the observations will not be repeated here. However, it is useful to give a brief overview of the study and to highlight the main conclusions which were drawn from the observations.

(i) *Synoptic situation.* A surface anticyclone was centred over the Atlantic, just west of Ireland, so that the flow across the Azores region was north-easterly. 1000 mb isobaric back trajectories and isentropic back trajectories from 700 mb for the 72 hours leading up to the start of the experiment confirmed that this experiment took place almost entirely in a continental airmass which had passed over north-west Europe.

(ii) *Observations.* The main observations made during this study can be summarized as follows:

(a) The cloud layer appeared to be decoupled from the surface, and four distinct layers were identified using the terminology described above (see Martin et al. (1995),
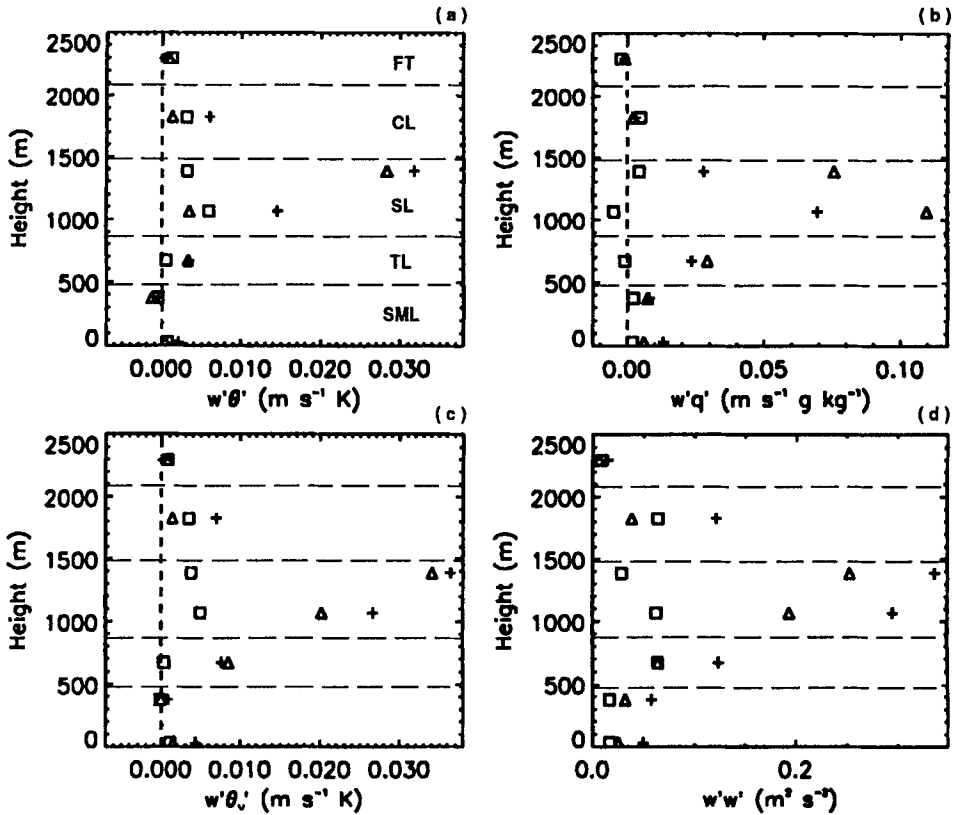
Figure 1. Turbulent-flux profiles obtained from a vertical stack of horizontal runs in the boundary layer during flight A213 on 19th June, 1992. (a) $w'\theta'$ (m s^{-1}K); (b) $w'q'$ (m s^{-1}g kg^{-1}); (c) $w'\theta'_v$ (m s^{-1}K); (d) $w'w'$ (m^{2}s^{-2}). $+$ = flux averages over each run; $\triangle$ = contribution from updraughts larger than one standard deviation of the w time-series for each run; $\square$ = contribution from downdraughts larger than one standard deviation of the w time-series for each run. The extent of each of the layers in the boundary layer (as defined in Martin *et al.* 1995) is shown by the long dashed lines. FT = free tropospheric air; CL = cloud layer; SL = sub-cloud layer; TL = transition layer; SML = surface-based mixed layer.

Figs. 5 and 6). The SML and sub-cloud layer were separated by a transition region in which the total water content (q_T) and equivalent potential temperature (θ_e) were both variable but generally decreased with height. Cumulus clouds were observed below the stratocumulus, with their bases close to the SML top. Many of these clouds rose into the stratocumulus layer above, and were associated with upward transport of air from the SML into the stratocumulus cloud layer.

The layered structure of the boundary-layer and the transport between the layers are further illustrated in Fig. 1. The plus signs ($+$) are fluxes of sensible heat ($w'\theta'$), latent heat ($w'q'$), buoyancy ($w'\theta'_v$), and vertical velocity ($w'w'$), derived (using the method described by Rogers *et al.* 1995) from turbulent velocity, temperature and humidity mixing-ratio measurements made at 32 Hz during ten-minute straight and level runs in the boundary layer and free troposphere (at 100 m s^{-1}) between 0820 and 0954 GMT on 19 June 1992. The uncertainty in the flux values is thought to be between 10–20%. The triangles ($\triangle$) show the contribution made by the stronger updraughts to the total flux at each level, and the squares ($\square$) show the contribution from the stronger downdraughts. These were derived using an eddy-correlation technique.

'Stronger' is defined in this case as being where the vertical velocity exceeds ±1 standard deviation of the average vertical velocity at each level. These contributions can give an indication of the main vertical transports within the boundary layer. However, it should be noted that the contribution from the stronger updraughts and downdraughts to the total flux averaged over the whole run will depend to some extent on how frequently such updraughts and downdraughts were encountered during the run, as well as on the magnitude and sign of the contributions from other scales. Similarly, the total average flux for a run through a sub-cloud layer in which cumulus clouds exist may vary according to the number of cumuli encountered by the aircraft, and this is likely to be different for runs at different heights in the boundary layer. These factors must be considered when interpreting the flux profiles in Fig. 1.

The top of the SML can be identified at around 400 m in Fig. 1, where there is a minimum in the fluxes of buoyancy and of sensible and latent heat. The region between 400–2080 m contains the transition, sub-cloud and cloud layers, and the approximate vertical extent of the stratocumulus layer is indicated. The vertical-velocity variance is a maximum in the sub-cloud layer, with a large contribution from the stronger updraughts. These are likely to be associated with the cumulus clouds growing through this layer from the top of the SML. The large positive contribution from the stronger updraughts to the sensible and latent-heat and buoyancy fluxes below the stratocumulus suggests that the cumulus clouds are responsible for significant transport of heat and moisture within this layer. Within the cloud layer the vertical-velocity variance is smaller than in the sub-cloud layer, since the vertical velocities associated with the stratocumulus are much weaker than those in the cumulus clouds, and the cumulus clouds which penetrate the stratocumulus are likely to be decelerating as a result of entrainment of unsaturated air below the stratocumulus base. There are still significant fluxes of buoyancy and of sensible and latent heat in the cloud layer, but now the largest contribution is from the stronger downdraughts. This may be an indicator of longwave radiative cooling from the cloud top. The cloud-top cooling rate early on 19 June 1992, calculated using the radiation model of Edwards and Slingo (1996) (J. P. Taylor, personal communication) was about 170 K day^{-1}, which is consistent with values from radiatively driven stratocumulus layers described by Nicholls and Leighton (1986) and Slingo et al. (1982).

(b) The cumulus clouds mainly formed in clusters of the order of 30 km diameter below the stratocumulus. This resulted in significant spatial variations in the characteristics of the stratocumulus, between regions where clusters of cumulus clouds were interacting with the layer, and the intervening regions.

(c) The stratocumulus layer was thicker in regions where cumulus clouds penetrated, and it was suggested by Martin et al. (1995) that this was due to the cumulus clouds merging with and spreading out into the cloud layer.

(d) The vertical extent of the stratocumulus layer also varied temporally during this Lagrangian study. During the afternoon and evening of 19 June 1992, the stratocumulus thinned and large breaks appeared, but the cloud persisted through the night so that a thin, patchy layer remained on the morning of 20 June. Additionally, the number of cumulus clouds large enough to penetrate the stratocumulus layer decreased substantially through the afternoon of 19 June 1992, reaching a minimum in the early morning of 20 June so that by 0600 GMT none of the cumulus cloud tops were reaching the stratocumulus base, and then increased again through the day.

(e) The intrusion of cumulus clouds into the stratocumulus layer resulted in localized increases in droplet concentration (from about 250 cm^{-3} to 500 cm^{-3}) and liquid-water content (LWC) (from 0.3 g m^{-3} to 0.75 g m^{-3} at the level at which the measurements
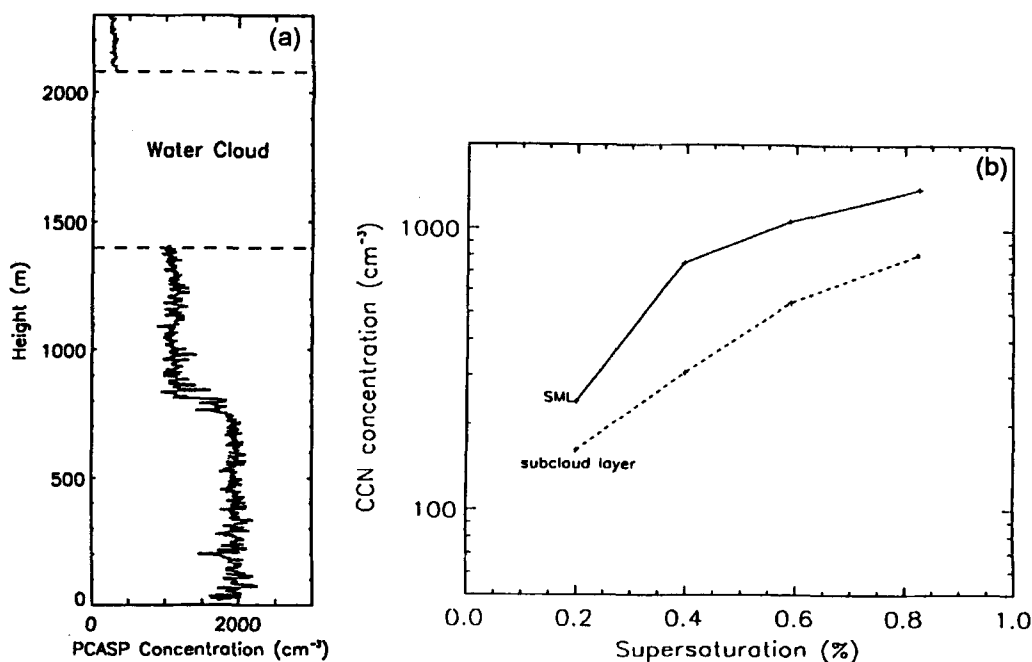
Figure 2. (a) Aerosol concentration measured with the PCASP probe during a profile through the boundary layer on 19 June 1992. Measurements made in cloud have been omitted from the profile due to instrument problems in cloud. (b) CCN activity spectra measured in the SML on 19 June at a height of 30 m (solid line) and in the sub-cloud layer at a height of 1380 m (dashed line). (Taken from Martin *et al.* (1995), Fig. 12).

were made) in the stratocumulus cloud layer. Figure 2(a) shows a profile of aerosol concentration measured by the PCASP at 0810 GMT on 19 June 1992. The high concentrations (around 1950 cm^{-3}) of aerosol particles in the 0.1–3.0 μm diameter range within the SML show that this airmass was relatively polluted. The aerosol concentration decreases sharply to around 1100 cm^{-3} at 800 m, and comparison with Figs. 5(a) and 6(a) of Martin *et al.* (1995) reveals that this coincides with the top of the transition layer. Figure 2(b) shows CCN activation spectra (that is, the number of CCN activated at different supersaturations) measured in the SML and the sub-cloud layer on the morning of 19 June (taken from Martin *et al.* 1995). It can be seen that more CCN are activated at any supersaturation in the SML than in the sub-cloud layer. The higher vertical velocities in the cumulus clouds (up to 3.5 m s^{-1}, compared with around 0.5 m s^{-1} in the stratocumulus; Martin *et al.* 1995), combined with the higher CCN concentrations in the air entering the cloud, will therefore increase the droplet concentration near the cloud base in the cumulus clouds relative to that in the stratocumulus. Dilution resulting from entrainment of dry air from the environment may offset this increase to some extent at higher levels in the cumuli (Jonas 1995). It is suggested, therefore, that the increases in droplet concentration in the stratocumulus in the regions of cumulus penetration were a result of both the higher concentrations of CCN on which the cumulus cloud droplets formed and the higher vertical velocities. The increases in LWC will be partly a result of the lower cloud base of the cumulus clouds compared with the stratocumulus and partly due to the increase in q_T as air from the SML is transported into the cloud layer via the cumulus clouds.

(f) Comparisons of the effects of cumulus clouds of similar vertical extent on stratocumulus layers of differing thickness indicated that the variations in the stratocumulus microphysics that were associated with penetrating cumulus clouds depended to some extent on the difference in cloud-base height between the two clouds. This is because the size to which droplets can grow in both the cumulus clouds and the stratocumulus will depend not only on the droplet concentration and available water-vapour content, but also on the cloud thickness (since droplets will have more time to grow by condensation during their passage through a thicker cloud). Local decreases in the maximum cloud-droplet size were observed in the regions of cumulus penetration when the stratocumulus layer was relatively thick, whereas a local increase in the droplet size was observed when a cumulus cloud of similar size penetrated a much thinner stratocumulus layer.

(g) Drizzle was reduced in regions of active cumulus penetration, compared with the surrounding stratocumulus, in this polluted airmass (Martin et al. 1995). This is thought to be a result of the overall decrease in droplet size associated with the increases in droplet concentration in the penetrating cumulus clouds.

(h) The optical depth of the stratocumulus cloud was greater in the vicinity of the cumulus cloud penetration. Increases in cloud optical depth may be due to an increase in the liquid-water path, or a decrease in droplet effective radius, or both (Slingo and Schrecker 1982; Fouquart et al. 1990; Slingo 1990). Both changes were observed in the aircraft data during this experiment.

(b)   Flight H812

(i)   *Synoptic situation.*   This flight was carried out on 16 July 1987, as part of FIRE, off the coast of San Diego, California. The synoptic situation is shown in Fig. 3(a). A high-pressure region to the north resulted in a north-north-westerly airflow through the operating region (shaded box). The flight track of the C-130 aircraft is shown in Fig. 3(b). A vertical stack of horizontal runs was carried out between $33.0°$N $120.66°$W and $33.6°$N $120.66°$W. This was planned to coincide with the 1800 GMT (1100 local) Landsat overpass at $33.2°$N $120.5°$W. The NCAR *Electra* was also flying at this time, with a flight track centred to the east of the C-130, marked 'X' on Fig. 3(b). Forecast trajectories, initialized on 15 July for parcels forecast to reach 925 mb at various locations at 0000 GMT on 16 July (Fig. 3(c)), indicate that the airmass may have been mainly maritime in origin. However, Hudson and Frisbie (1991) stated that back trajectories calculated from the *Electra*'s position indicated a recent passage over land for this air which was about 100 km from the coast. Although the C-130 was flying about 100 km west of the *Electra*'s position, it is possible that the airmass sampled in this study may have picked up some anthropogenic influence.

(ii)   *Structure of the boundary layer.*   Figure 4 shows data from an ascent through the boundary layer at $33.6°$N $120.66°$W. Also plotted on the θ_e and q_T profiles are the average and range of values measured during each of the horizontal runs at different heights. The difference between the values of θ_e and q_T measured during the ascent and those measured during the horizontal runs indicates the degree of lateral variability within this boundary layer. The boundary layer is shallow, with the temperature inversion at 760 m, and the stratocumulus layer extends down to 430 m, as shown by the LWC profile. The aircraft also passed through cloud below the stratocumulus base during this slanted profile. It is not clear from Fig. 4 whether this is a second stratocumulus layer or whether it is a cumulus cloud and the aircraft has passed into one side of the cloud at 230 m and out of the other side at 370 m. Visual observations made during the flight suggest that the lower cloud
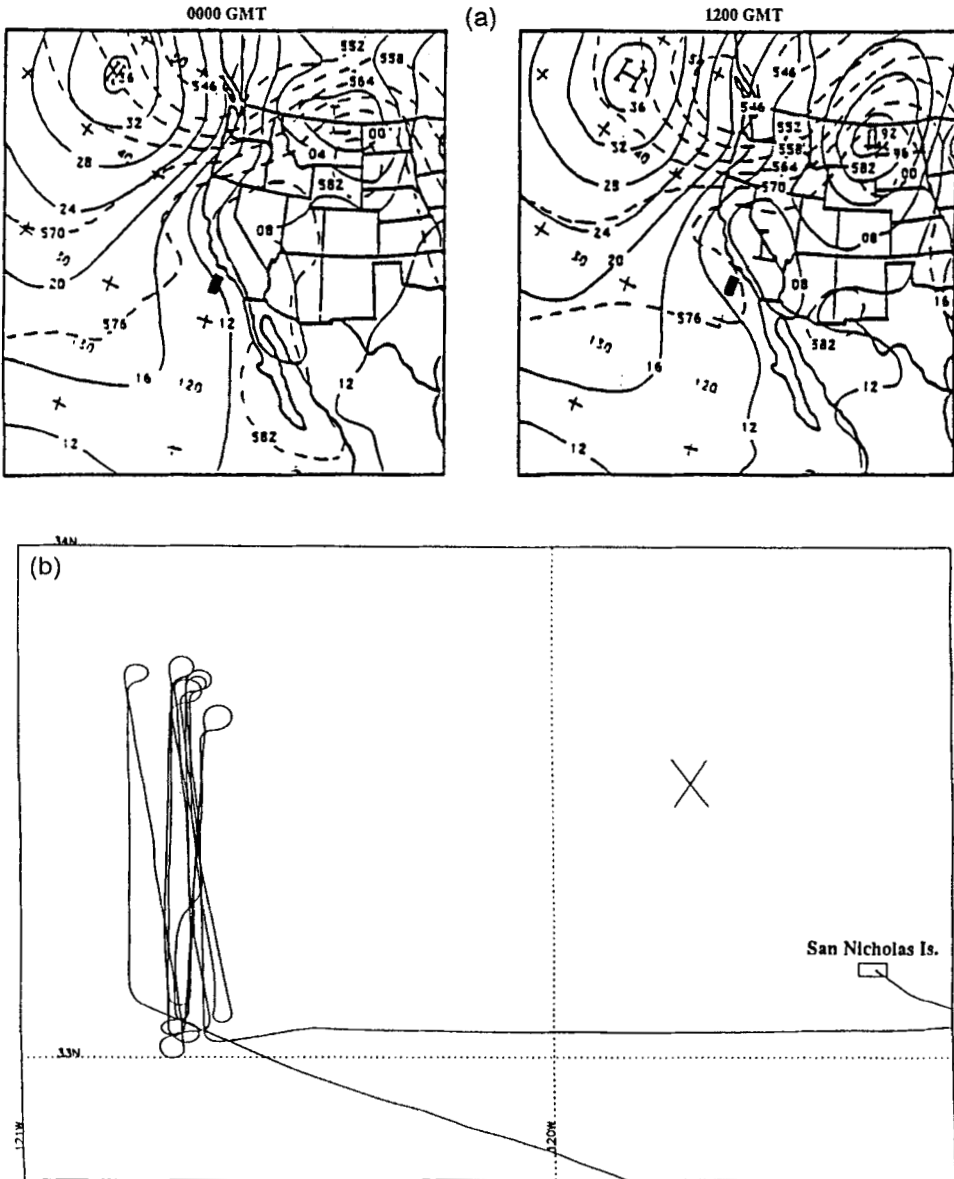
Figure 3.   (a) Synoptic situation in the FIRE experimental region (indicated by the shaded box) on 16 July 1987, at 0000 GMT and 1200 GMT. (b) Flight track for the C-130 aircraft during flight H812 on 16 July, 1987, off the coast of California. The cross indicates the general operating area of the NCAR *Electra* aircraft at the same time. (c) 24-hour trajectory forecasts from NEPRF's Naval Operations Regional Atmospheric Prediction System model initialized at 0000 GMT on 15 July 1987 (original pressure level (mb) and location given) for air parcels forecast to reach 925 mb at various locations at 0000 GMT on 16 July, 1987. (From Kloesel *et al.* (1988)).
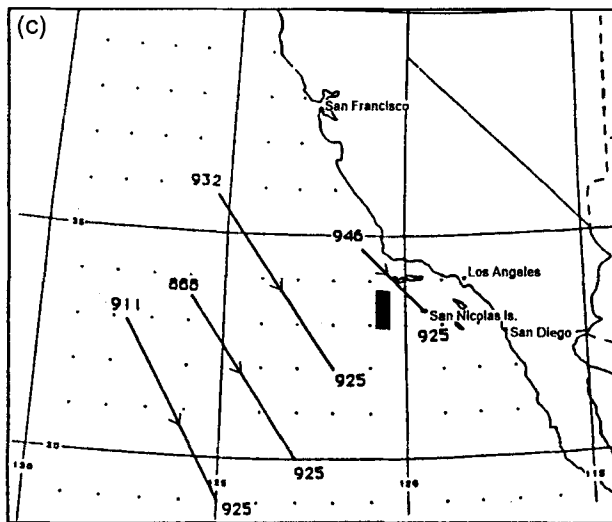
Figure 3.   Continued.
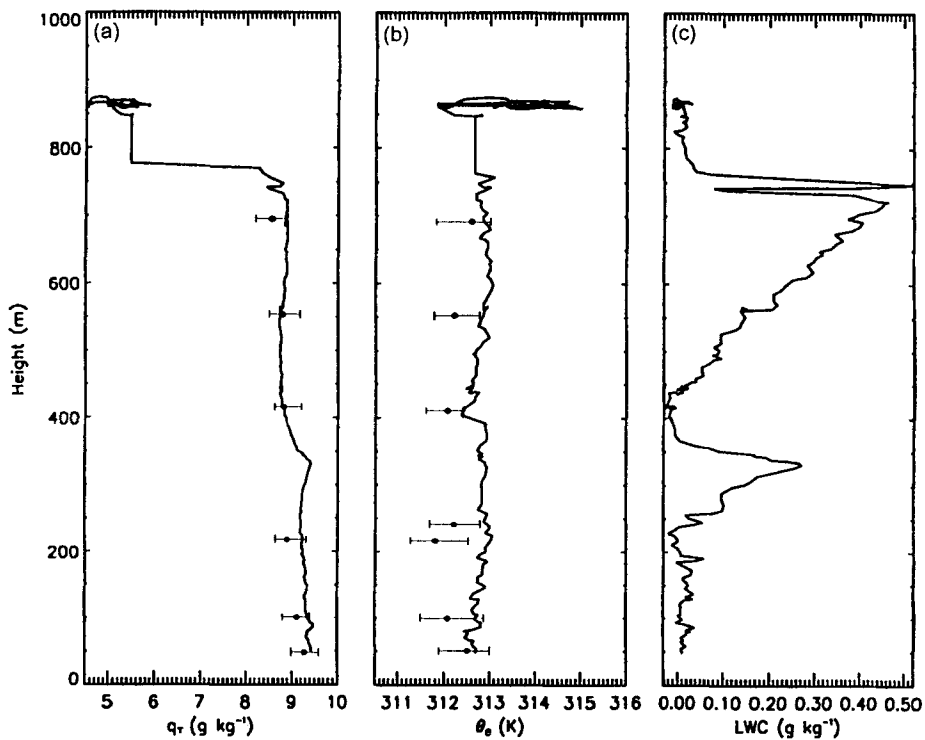
Figure 4.   Profiles of q_T, θ_e and liquid-water content (LWC) measured during an ascent through the boundary layer at 33.6°N 120.66°W on 16 July, 1987. The points show the average values measured during the stack of horizontal runs, and the bars indicate the range of values measured during each run.
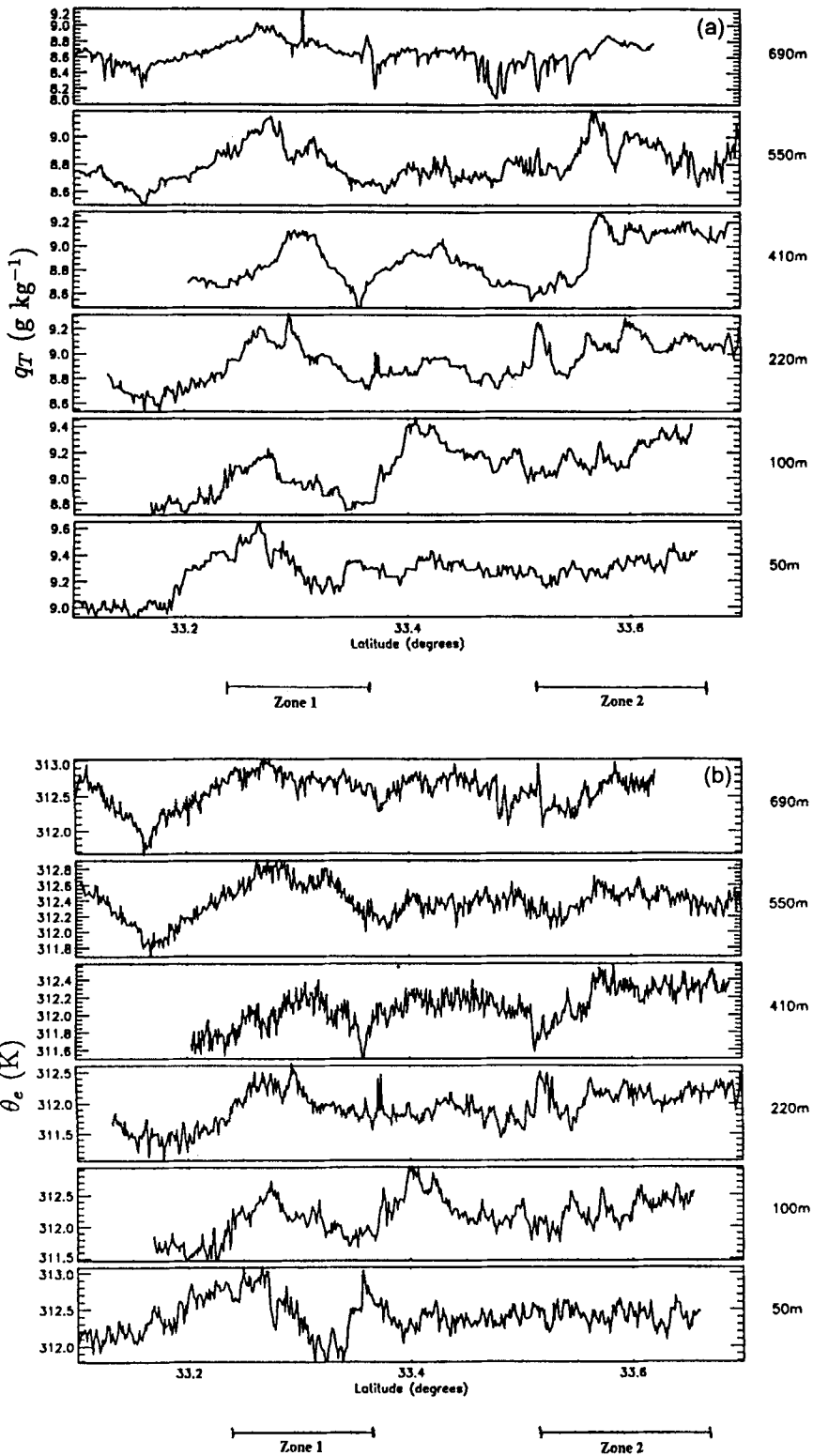
Figure 5. Measurements made during the stack of horizontal runs on 16 July 1987. Two zones of cumulus penetration, identified as in the text, are shown. (a) q_T (g kg^{-1}); (b) θ_e (K); (c) LWC (g m^{-3}); (d) w (m s^{-1}).
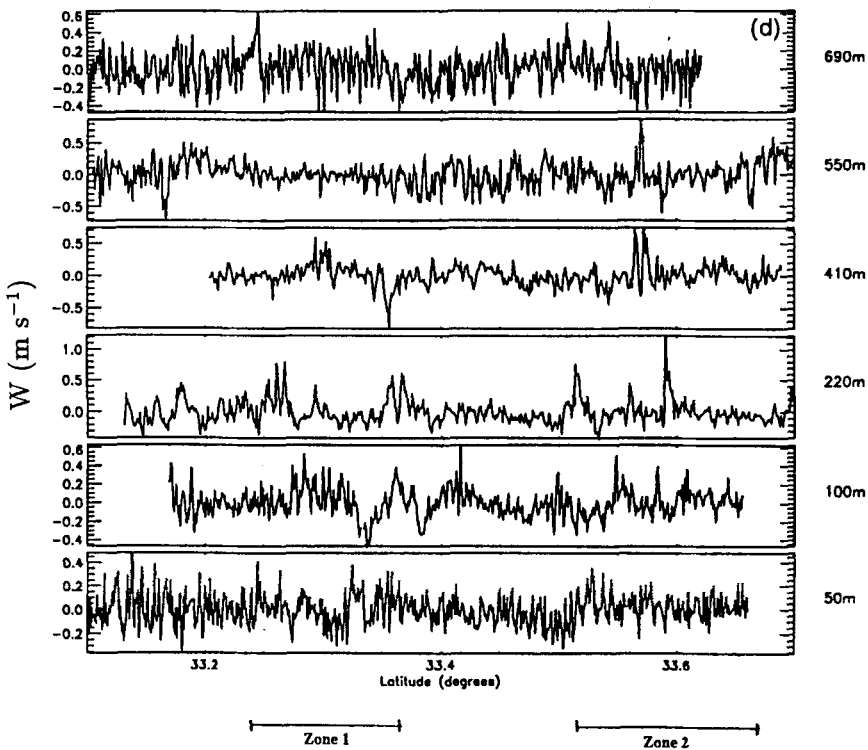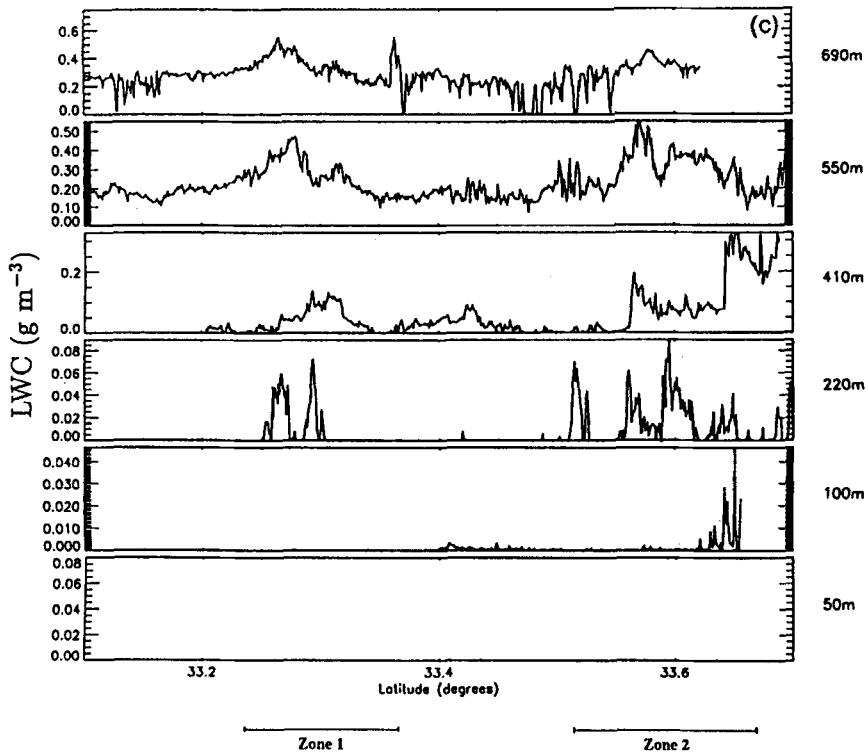
Figure 5.   Continued.
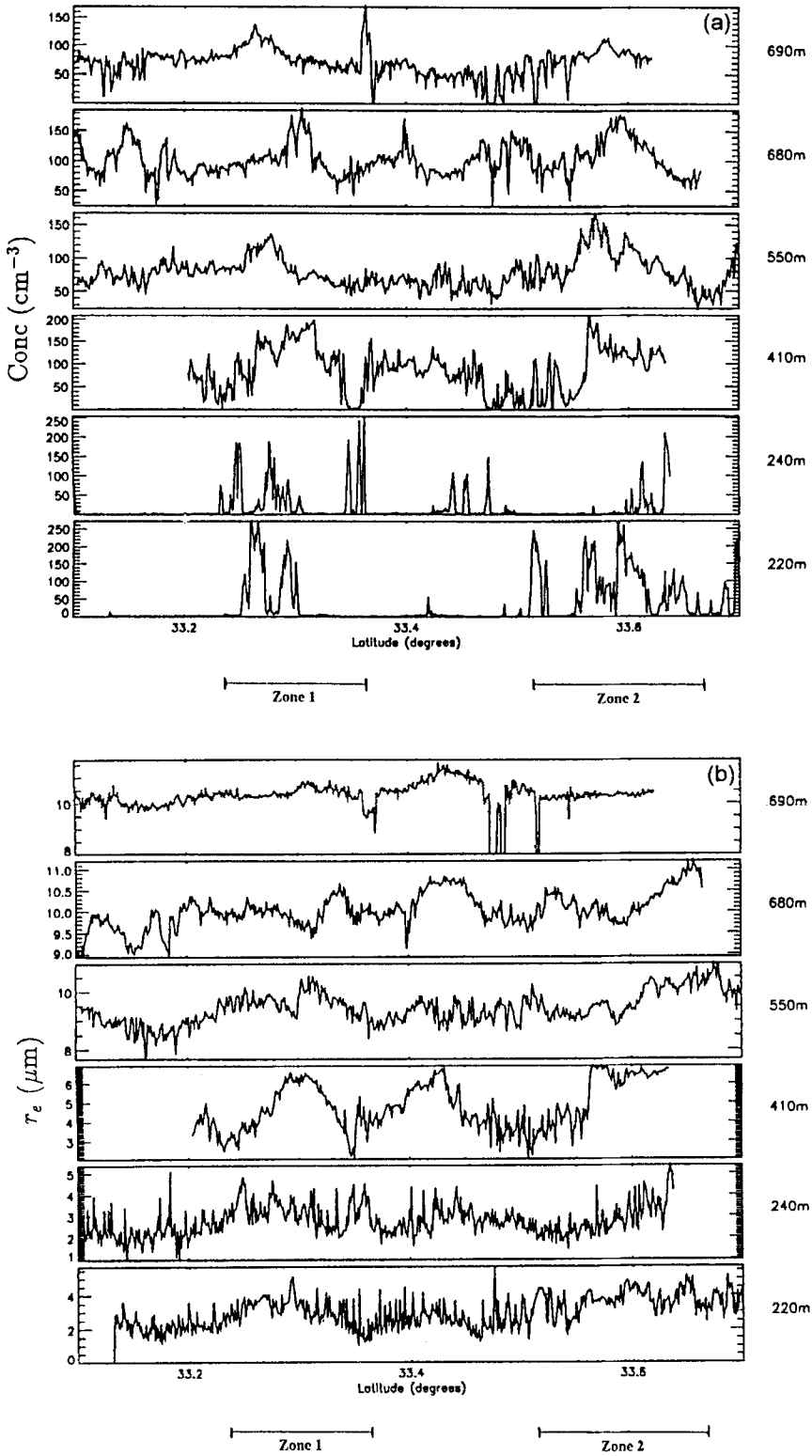
Figure 6.   Microphysical measurements made during six horizontal runs in the boundary layer. Those at 550 m, 680 m and 690 m are through the stratocumulus layer and the other two are below the stratocumulus. (a) droplet concentration (cm^{-3}); (b) r_e (μm).
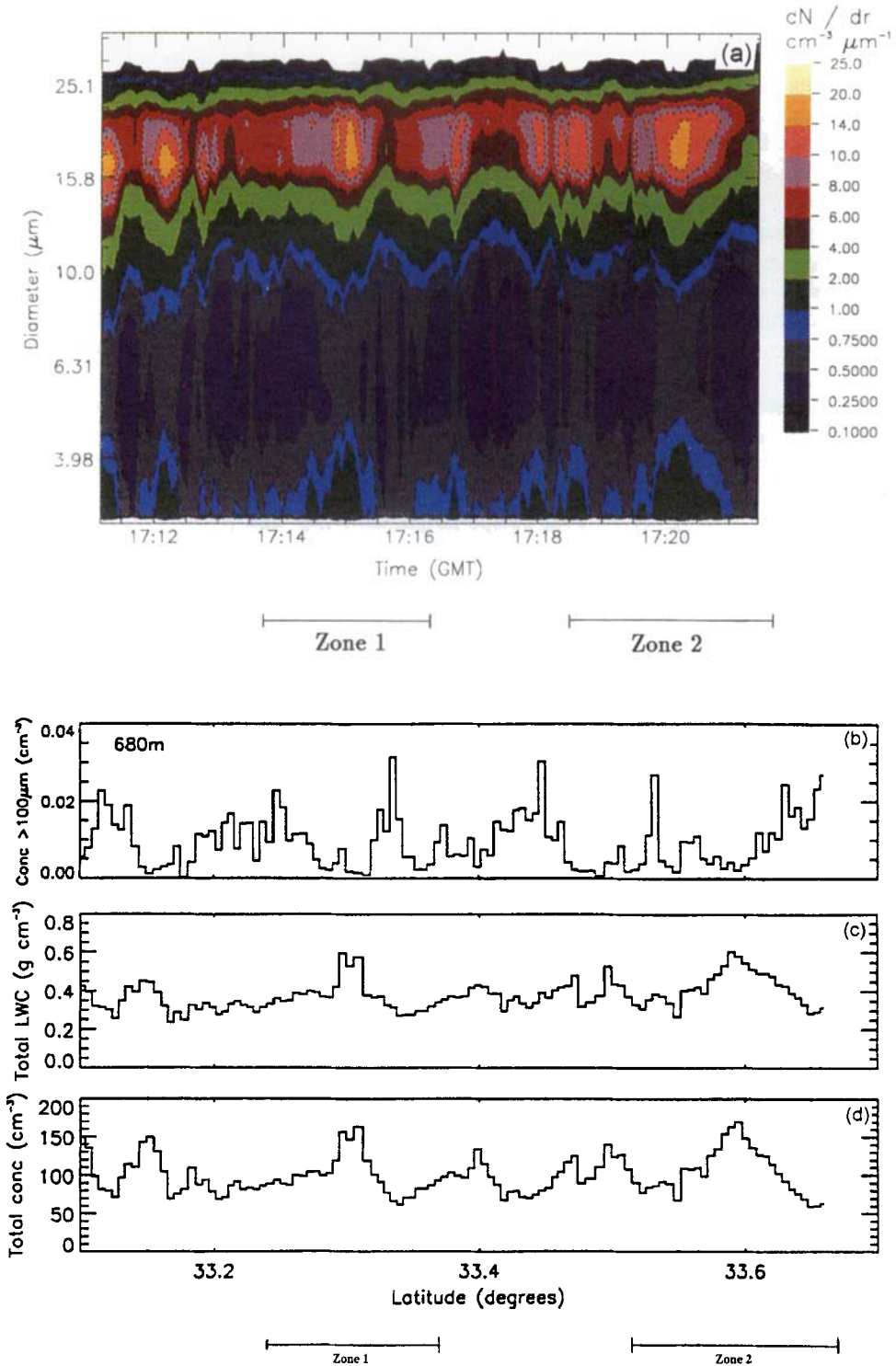
Figure 7.   (a) Contoured droplet spectra measured by the FSSP during a horizontal run through the stratocumulus at 680 m on 16 July 1987, averaged over 5-second intervals. The zones of cumulus-cloud penetration identified in Fig. 5 are shown. (b) Concentration of droplets larger than 100 μm diameter measured during the run in (a); (c) and (d) Total LWC and droplet concentration obtained by combining 5-second averages of measurements from the FSSP and 2DC probes during the run in (a).

occurred as patches of stratus fractus, with occasional cumuli managing to grow into the upper cloud layer. However, no video recording of the cloud conditions was made during this flight, and it is therefore difficult to confirm the type of cloud sampled during this aircraft ascent. It is possible that the lower cloud region seen in Fig. 4 may be a combination of the stratus fractus and a larger cumulus cloud.

The vertical variations in q_T and θ_e are small in the boundary layer as a whole, but there is some indication that the region below the lower cloud has a larger q_T than the region in which the stratocumulus layer exists. This suggests that the boundary layer is not well-mixed vertically. Additionally, the existence of cloud below the stratocumulus layer and separate from it implies that vertical transport of moisture from the sea surface up to the stratocumulus layer is being inhibited, such that moisture can build up at lower levels until saturation occurs. We term this layer the SML even though the layer does not appear to be as well-mixed as the other cases described in this paper. Turbulent-flux measurements obtained from the stack of horizontal runs in the boundary layer were an order of magnitude smaller in this case than in the Lagrangian study described in section 3(a), and it was difficult to pick out any vertical structure. Consequently, the flux measurements are not shown here.

Figures 5(a) to (d) show time-series of q_T, θ_e, LWC and vertical velocity, for six horizontal runs in the vertical stack. Each is plotted against latitude (since the runs were approximately along a line of longitude) and the height of each is shown. The runs at 50 m and 100 m were below all cloud, and that at 220 m passed through both active and decaying cumuli. The run at 410 m was just at the base of the stratocumulus layer, the run at 550 m at mid-level in the cloud, and the run at 690 m was close to the stratocumulus top. It is apparent that the average q_T values in the runs at 220 m and above are lower than those from the runs at 50 m and 100 m (which were probably in the SML), but that there are regions in each run where the q_T approaches or exceeds $9.2\,\mathrm{g\,kg^{-1}}$. The cumuli encountered during the run at 220 m can be identified from comparisons between the vertical-velocity and liquid-water-content time-series (Figs. 5(c) and (d)), which show updraughts of up to $1.2\,\mathrm{m\,s^{-1}}$ coinciding with some of the cloud penetrations. Comparison with Fig. 5(a) reveals that these updraughts are also associated with increases in q_T to values which are similar to those in the SML.

That these are cumulus clouds rather than the lower stratus fractus may be ascertained by tracing these updraughts up into the stratocumulus. Although each run took ten minutes and the aircraft was therefore making observations in the stack for about three hours, the horizontal winds were very light (60 km run averaged winds were less than $2\,\mathrm{m\,s^{-1}}$ at all levels). However, it is unlikely that an individual cumulus cloud could be traced vertically between the runs because of their short life-times ($\sim$ minutes, Jonas 1996). In order to try to characterize the regions of penetrative convection, two main 'zones' have been selected from the aircraft track, each covering a region where cloudy updraughts were sampled below the stratocumulus. The extent of each is shown in Fig. 5. The more southerly will be referred to as Zone 1 and the other as Zone 2.

It is apparent from Fig. 5((a) and (c)) that the zones of cumulus activity are associated with increases in q_T and LWC in the overlying stratocumulus. This suggests that the cumulus clouds are penetrating the stratocumulus and transporting moisture from the SML into the stratocumulus layer. There is also some indication of an increase in θ_e but this is not as clear as the change in q_T and LWC. It is interesting to note that the increases in LWC and q_T within the zones are not always accompanied by updraughts in the vertical-velocity time-series (Fig. 5(d)). It is possible either that the aircraft did not pass through the updraught regions of the cumulus clouds with which the increases are associated, or that the updraught has begun to decay but its effects remain in the upper cloud layer. The

latter possibility could have important implications for the subsequent evolution of the cloud layer.

(iii) *Cloud microphysics.* Figure 6 shows time series of droplet concentration and droplet effective radius for six runs in the boundary layer, four of which were shown in Fig. 5. The zones of cumulus penetration identified in section 3(b)(ii) are also shown in Fig. 6. It is apparent from the runs through the stratocumulus layer (at 550 m, 680 m and 690 m) that the cumulus cloud penetrations are associated with increases in the droplet concentration, but that there is little change in the droplet effective-radius in the zones compared with that in the surrounding stratocumulus. These measurements imply that whilst the penetrating cumulus clouds are carrying moisture up into the cloud layer from the SML and hence increasing the LWC, they also have a higher droplet-concentration, such that the average droplet size in these clouds is similar to or slightly smaller than that already existing in the stratocumulus. It should be noted that care must be taken when comparing the actual droplet concentrations, effective radii and LWCs (Fig. 5(c)) in the runs at 220 m, 240 m and 410 m with those in the runs at 550 m, 680 m and 690 m because the range of droplet sizes accepted and counted by the FSSP was altered from 1–16 μm to 2–32 μm diameter after the run at 410 m. It is impossible to estimate the contribution of this change to the differences in the droplet concentrations, effective radii and LWC between the runs in the stratocumulus and those below it. However, the runs below the cloud layer are used here simply to illustrate the presence and location of the cumulus clouds, so we do not consider that this instrument change affects the conclusions drawn from these measurements.

It cannot be determined from the available aircraft observations to what degree the higher droplet-concentrations in the cumulus clouds were affected by the aerosol concentrations in the boundary layer. Although there was no aerosol-measuring capability on the C-130 aircraft during this experiment, measurements of condensation nucleus (CN) and CCN concentrations were made on the *Electra* aircraft on this day, and are reported in Hudson and Frisbie (1991). These suggest a CN concentration of 200–400 cm^{-3} at about 50 m, with a corresponding CCN concentration of 150–350 cm^{-3} (for all CCN active at 1% supersaturation), but there is no indication of a significant change in CCN concentration with height in the boundary layer. It is unlikely that the airmasses sampled by the two aircraft were exactly the same, since the C-130 was 100 km further west and the general airflow was from the north-west, so the concentration of CCN in the airmass sampled by the C-130 may have been larger in the SML than the subcloud layer below the stratocumulus. However, it may be that, in this case, the increased droplet concentrations in the cumulus clouds were mainly due to the larger updraught velocities causing more CCN to be activated.

Figure 7(a) shows contoured droplet spectra measured during the run at 680 m through the stratocumulus. The zones of cumulus-cloud penetration are marked, and the increases in droplet concentration within these zones can be seen clearly. However, there is no clearly defined change in the spectral shape between the zones and the surrounding stratocumulus. There is some indication of bi-modality in the spectra within the zones, with a second peak at small sizes and mostly out of the range of the FSSP. However, it is clear that the microphysical change is more in droplet concentration than droplet size. This also implies a change in LWC.

Figure 7(b) shows approximately 5-second averages* of the concentration of drops larger than 100 μm diameter, measured with the 2D Cloud probe during the run through the

---

* The 2DC probe records drop images (see section 2) in data buffers which must be filled before they are sent to the data-recording system. At low drop-concentrations it may take several seconds or even minutes before the data buffer is filled, so that the resolution of the measurements is limited by the actual drop concentration.
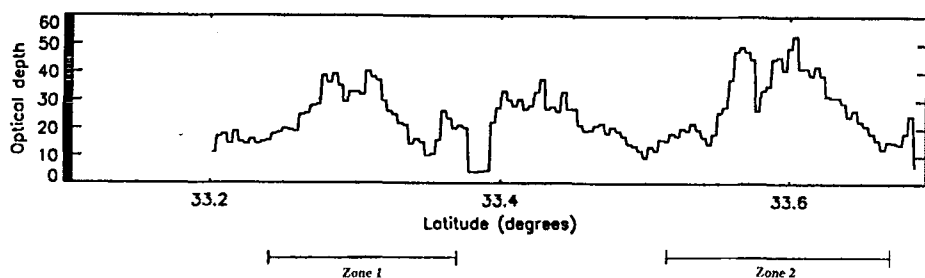
Figure 8. Cloud optical depth obtained from measurements made by a multi-channel radiometer during a run above the cloud top on 16 July 1987.

cloud in Fig. 7(a). The averaging is used in order to increase the volume of air sampled for each measurement, due to the relatively smaller concentrations of drizzle-sized droplets. There is no definite increase or decrease in the concentration of these drizzle-sized drops between the zones as a whole and the surrounding regions. However, comparison with Figs. 7(c) and (d), which show the LWC and total droplet concentration for both cloud and drizzle-sized droplets (obtained by combining measurements from the FSSP and 2DC probes) reveals that decreases in the drizzle-drop concentration within the zones are generally correlated with sharp increases in the total droplet concentration and LWC. This implies that the increases in droplet concentration, which it has been suggested are associated with cumulus cloud penetrations, may result in a decrease in the number and size of drizzle drops locally.

(iv) *Remote sensing of cloud properties.* Figure 8 shows a time-series of cloud optical depth retrieved from narrow-band measurements at 1.04 μm wavelength which were made using a multi-channel radiometer (MCR) during a run above the cloud layer (Taylor 1992; Rawlins and Foot 1990). The optical depth increases to more than 40 in the zones of cumulus penetration, from a background value of about 18. There is also a region of increased optical depth between 33.4 and 33.45 degrees latitude. Although this is not in one of the major zones of cumulus penetration, the run at 240 m in Fig. 6 shows that there were cumulus clouds below the stratocumulus in this region, and it is possible that these contributed to the total liquid-water path and hence the optical depth in this region.

Figure 9 shows a Landsat Band-4 reflectivity image recorded at 1800 GMT. Band-4 corresponds to 0.76–0.90 μm and falls into the shortwave part of the spectrum, which is more sensitive to changes in liquid-water path than to changes in cloud-droplet size. The position of the aircraft stack is shown, along with the zones of cumulus penetration identified from the aircraft observations. It is apparent that the zones coincide approximately with maxima in the reflectivity at these wavelengths, indicating increases in the liquid-water path in these regions. This is in good agreement with the variation in optical depth retrieved from the aircraft observations and with the observations of the cloud structure made in the boundary layer during the flight.

Comparison of Figs. 5(c) and (d), and Fig. 6(a), with Fig. 9 reveals that the radiative properties of the cloud vary more smoothly than the changes in droplet concentration, LWC and vertical velocity (note that the spatial resolution of the Landsat image shown in Fig. 9 is about 90 m, which is similar to that of the microphysical measurements from the aircraft at 1 Hz). This may be a compound effect of spreading of the penetrating cumulus clouds with height as they approach the stratocumulus top, and the presence of small cumuli below the stratocumulus layer which will contribute to the total cloud liquid-water path even if they do not penetrate the stratocumulus layer itself. It is apparent from Fig. 9 that
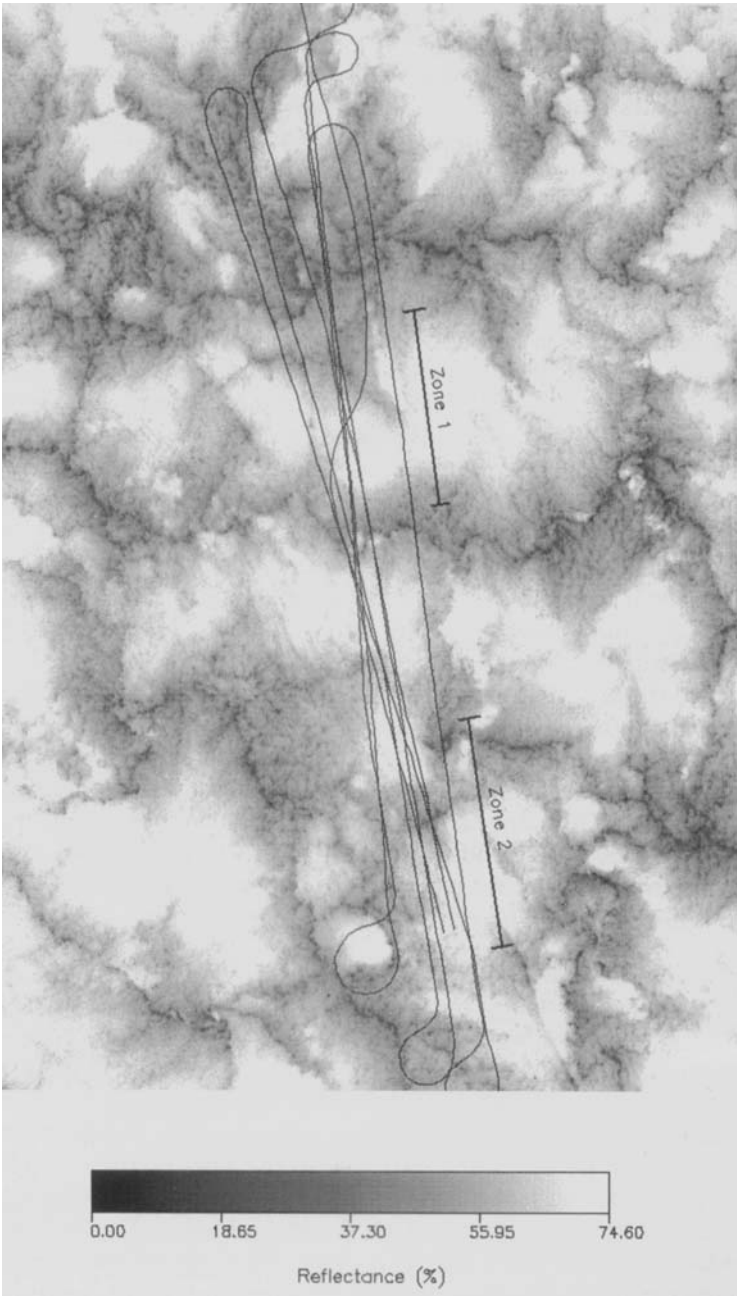
Figure 9.   Cloud reflectance at 0.76–0.90 μm wavelength measured during a Landsat overpass of the operating region at 1800 GMT on 16 July 1987. The flight track of the C-130 aircraft is shown, with the zones of cumulus penetration as defined from the aircraft measurements. The image resolution is 90 m.

there is another region of increased reflectance between the zones of cumulus penetration observed from the aircraft. This was also seen in the aircraft measurements of optical depth in Fig. 8 and, as suggested above, may be a result of the increased liquid-water path due to the cumulus clouds beneath the stratocumulus. The satellite image in Fig. 9 also reveals that similar variations in cloud optical depth exist across the whole of the region shown in the image. The NCAR *Electra* was flying to the east of the C-130 (see Fig. 3(b)) and also observed cumulus and stratus fractus below the stratocumulus layer (Paluch and Lenschow 1991). The suggests that the effects observed by the aircraft are quite representative of the area as a whole.

(c)   *Flight A005*

(i) *Synoptic situation.* This flight was carried out on 18 May 1990, over the North Sea. The flight pattern and location are shown in Fig. 10(a). A cold front had passed through the area during the previous day, behind which pressure was building. A high-pressure region was situated to the east of Iceland (see Fig. 10(b)), so that the North Sea was in a northerly airflow. The flight pattern consisted of two series of horizontal runs, each vertically stacked and oriented perpendicular to the wind direction, with one stack (A) in the south of the operating area and the other (B) in the north (see Fig. 10(a)). In order to trace the origin of the air in the operating area, isobaric back trajectories at 950 mb (in the boundary layer) were calculated from this region through the previous 48 hours, using the UK Meteorological Office model initialized wind-fields, and are shown in Fig. 10(c). The air does not appear to have passed over any land as it moved southwards to the operating area, and can therefore be termed a maritime airmass.

An extensive sheet of stratocumulus covered the North Sea and most of the United Kingdom, and, when viewed from the aircraft, was apparently quite uniform with few breaks and a very flat top. Much of the cloud layer was supercooled, with cloud-top temperatures varying from about $-1\,°C$ to $-2.5\,°C$. However, no ice particles were clearly identifiable in the images from the 2DC (which has a lower size limit of 150 μm diameter for images whose shapes can be identified; Moss and Johnson 1994). The possibility remains that there were smaller ice particles and water droplets existing together in the cloud. However, this seems unlikely at such temperatures.

(ii) *Structure of the boundary layer.* Figure 11 shows vertical profiles of q_T and θ_e from this flight. Also plotted on the θ_e and q_T profiles are the average and range of values measured during each of the horizontal runs in stack A. The profiles indicate that the boundary layer is not well-mixed vertically; a step change in each of the parameters can be seen at 540 m, with higher values in the SML. This suggests that the cloud layer is decoupled from the surface. During this flight, many cumulus clouds were observed to form with their bases at the top of the SML and to rise through the sub-cloud layer into the stratocumulus cloud. One such cloud was penetrated by the aircraft during this profile, as indicated in Fig. 11(b), and it can be seen that the values of q_T and θ_e in the cumulus cloud are similar to those in the lowest part of the SML. Values similar to those in the SML are also seen in the upper part of the stratocumulus layer in this profile. It is possible that, during the slanted ascent through the stratocumulus, a region of penetrating cumuli was encountered, and that the higher values of q_T and θ_e in the stratocumulus layer are associated with upward transport of air from the SML. Figure 11(b) shows that there is a small decrease in θ_e with height in the SML. This implies that this layer is conditionally unstable. It is possible that the cumulus clouds may have been transporting moisture out of the SML faster than the moisture flux from the sea surface could replace it, so that the layer
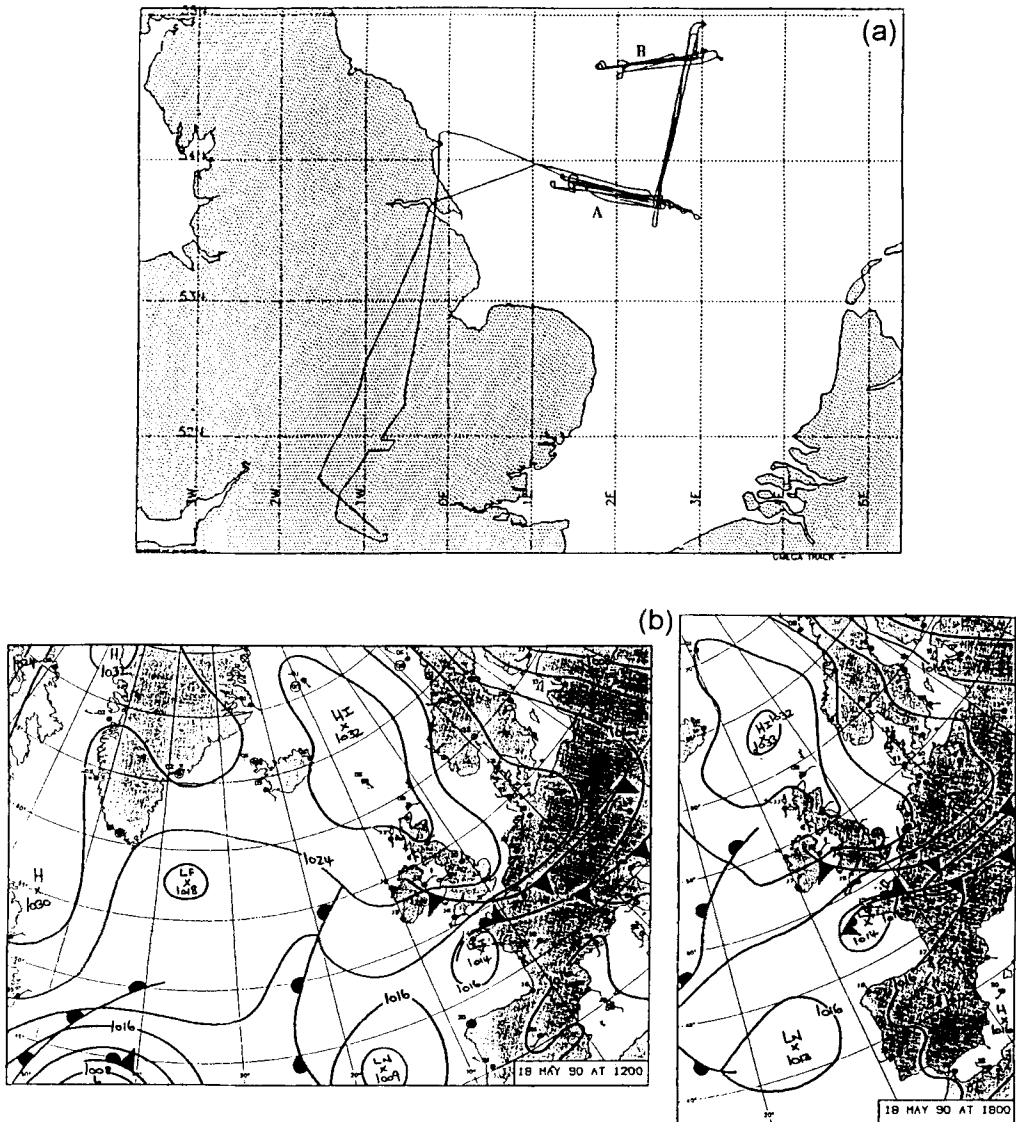
Figure 10.   (a) Flight track of C-130 aircraft during flight A005 on 18 May 1990. (b) Synoptic situation for flight A005 on 18 May 1990 at 1200 GMT and 1800 GMT. (c) Isobaric back-trajectories calculated at 950 mb from 1800 GMT on 18 May 1990, to 1800 GMT on 16 May 1990, using the UK Meteorological Office model. Arrowheads indicate every 6 hours.

was no longer well-mixed. Fluxes of sensible heat, moisture and buoyancy were calculated from measurements made during the horizontal runs in stack A. These were found to be considerably smaller than those from the Lagrangian study (Fig. 1), although they were slightly larger than those from H812. However, the vertical resolution of this stack of runs was poor, so that it was not possible to draw any conclusions about the vertical transports within the boundary layer from the fluxes.

Figure 12 shows the total aerosol concentration measured during the descent through the boundary layer shown in Fig. 11. There is little change in total aerosol concentration with height in the boundary layer, with a concentration of about 180 cm^{-3}. Above the inver-

Figure 10.   Continued.

Figure 11.   Profiles of (a) q_T and (b) θ_e measured in the boundary layer at 53.75°N 2.5°E during flight A005 on 18 May 1990. Dashed lines indicate the approximate limits of the different layers in the boundary layer.
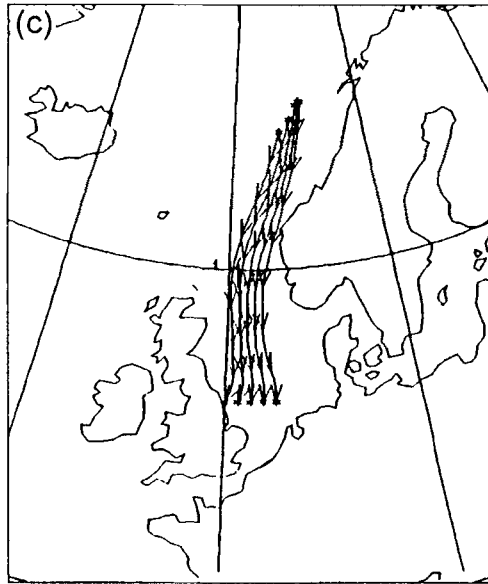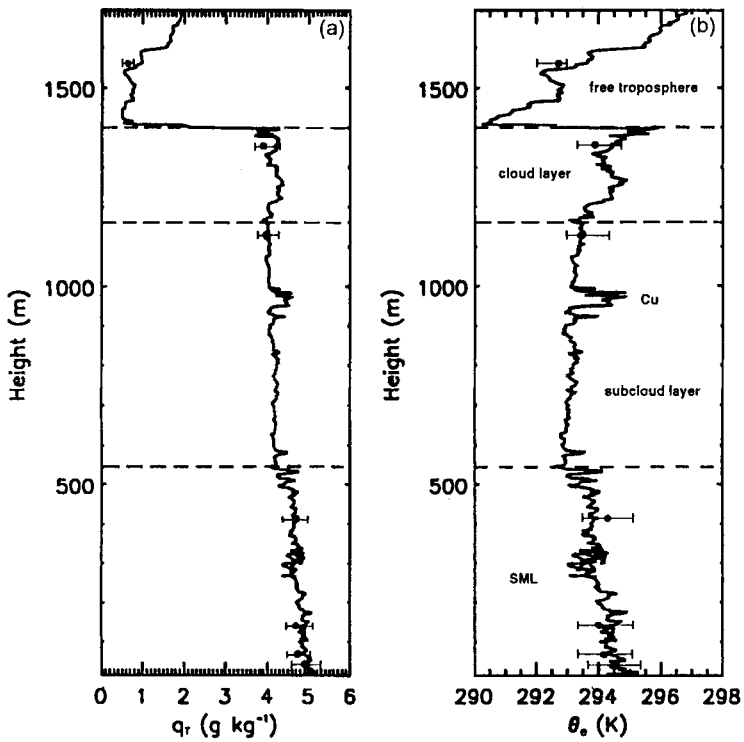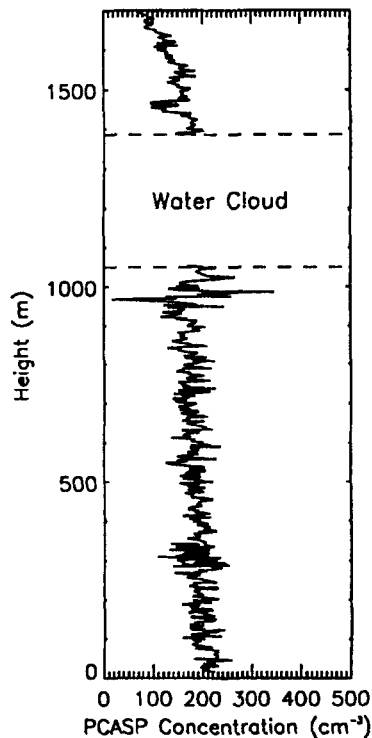
Figure 12. Aerosol concentration measured with the PCASP during a profile through the boundary layer at 53.75°N 2.5°E on 18 May 1990.

sion, the aerosol concentration remains between 100–180 cm^{-3}, but decreases with height. The aerosol concentrations in the boundary layer are relatively low, and characteristic of a clean airmass (Martin *et al.* 1994).

Figure 13 shows the values of q_T, θ_e, vertical velocity and LWC measured during two runs in stack A (see Fig. 10(a)). Each is plotted against distance from the same reference point, which is on the east side of the runs. The lower run (at 1135 m) was carried out about 100 m below the stratocumulus cloud base, and the upper run (at 1360 m) was through the middle of the stratocumulus layer. The runs were almost over the same ground positions (although they were about 15 minutes apart), and the winds were less than 5 m s^{-1} throughout the boundary layer. This implies that the cloud layer may have been advected a maximum of about 4.5 km between any two consecutive runs. However, the cumulus clouds observed during this flight were present in clusters of about 10–20 km in diameter and separated by about 10 km. Therefore, it is likely that a region of cumulus clouds sampled during the lower run can approximately be traced to the upper run.

The time-series of LWC (Fig. 13(d)) has been annotated using visual observations made during the lower run. Several cumulus clouds were sampled below the stratocumulus base (as seen from the time-series of LWC measured at 1135 m), some of which were merging with the stratocumulus layer and some of which were distinctly separated from it. Figure 13(a) and (b) shows that sharp increases in q_T and θ_e are associated with the cumulus clouds, both below and within the stratocumulus layer. Comparison with Fig. 11 reveals that these values of q_T and θ_e are similar to those measured in the SML during the profile, indicating that the cumulus clouds were transporting air from the SML through the sub-cloud layer and into the stratocumulus. However, the graphs of vertical velocity
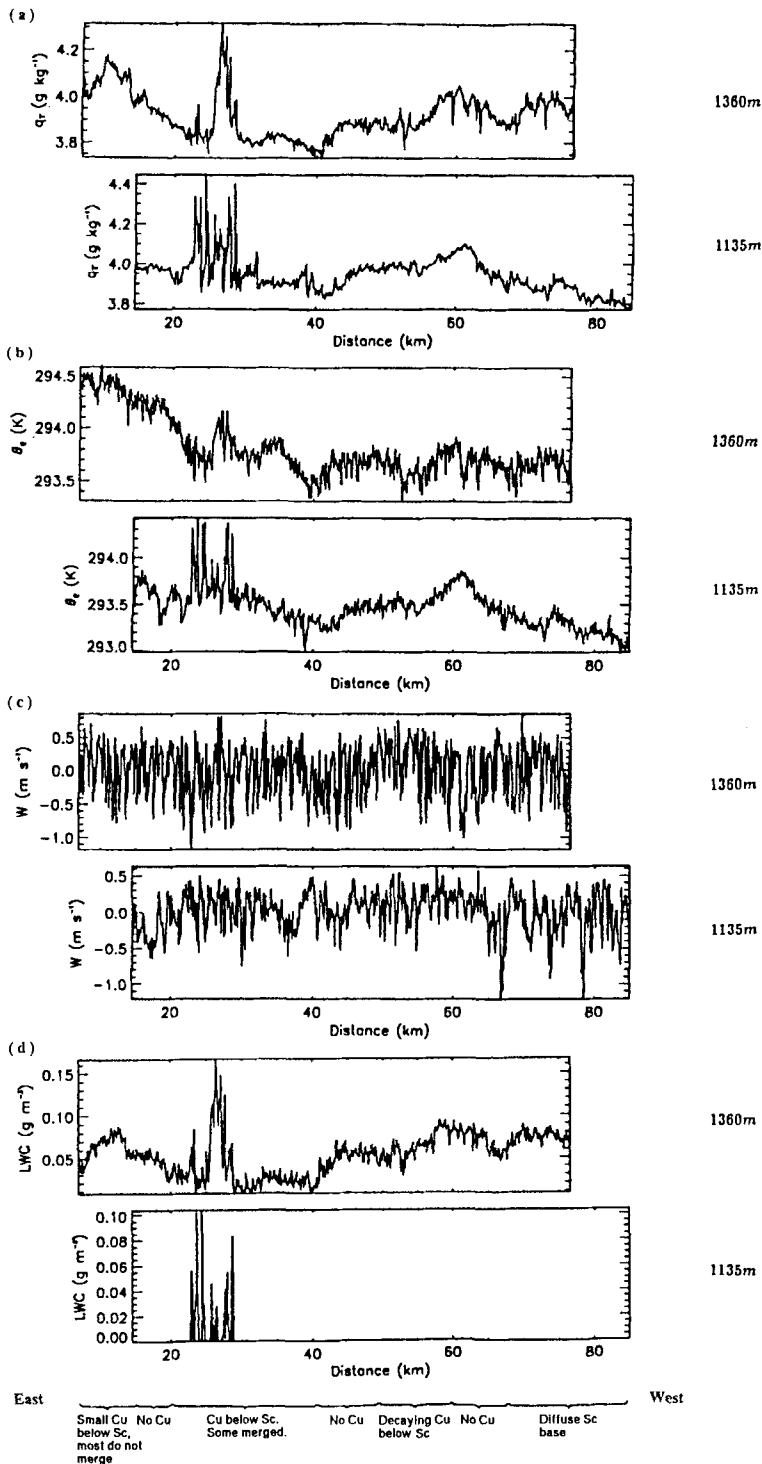
Figure 13.   Measurements made during two vertically stacked horizontal runs which were part of stack A on 18 May 1990, the upper one through the stratocumulus layer and the lower run just below the stratocumulus base. Each is plotted against distance from a fixed reference point at 53.66°N 2.80°E, which is at the eastern end of the runs. (a) q_T (g kg^{-1}); (b) θ_e (K); (c) vertical velocity, w (m s^{-1}); (d) liquid-water content (g m^{-3}).
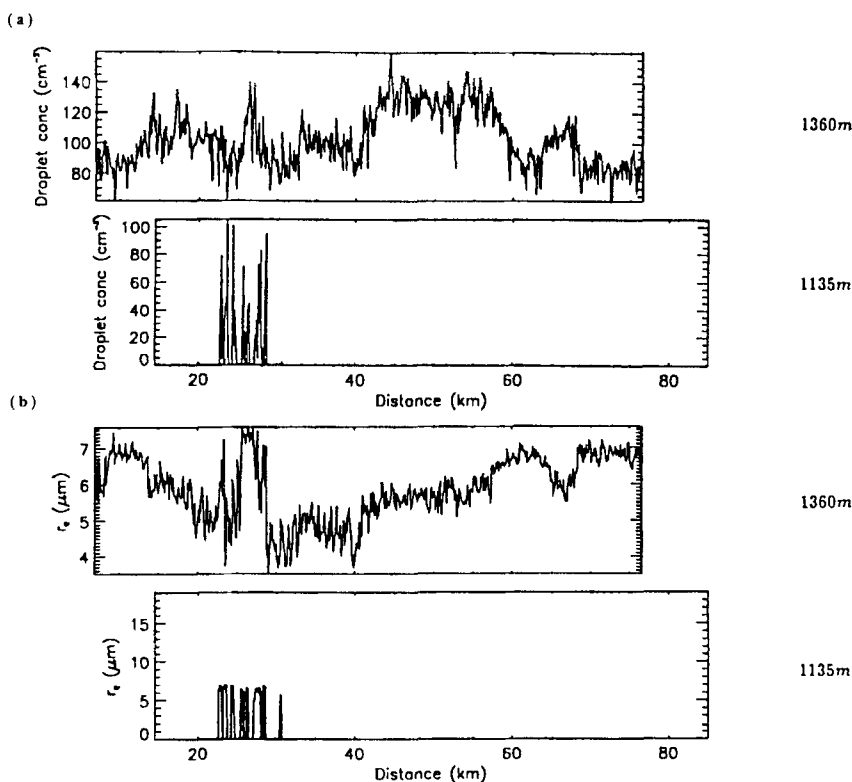
Figure 14.   As Fig. 13, but for (a) droplet concentration; (b) droplet-effective-radius.

show that the updraughts associated with these cumulus clouds were small. It is possible that the large increases in these thermodynamic parameters measured in the run through the stratocumulus were caused by a more active cumulus cloud which had since decayed. This suggests that the effects of penetrating cumulus clouds on the stratocumulus layer may persist even after the original updraughts have ceased.

(iii)   *Cloud microphysics.*   Figure 14 shows measurements of droplet concentration and effective radius measured during the two runs in Fig. 13. Although the stratocumulus sheet appeared quite flat and unbroken when observed from above, these measurements indicate significant inhomogeneities in the cloud microphysics. A sharp increase in droplet effective radius can be seen in the stratocumulus at about 27 km, and a smaller, but noticeable, increase in droplet concentration. Comparison with Fig. 13(d) reveals that these coincide with a sharp increase in LWC, and correspond to where the cumulus clouds were observed below the stratocumulus.

Figure 15 shows a contour plot of droplet-size spectra averaged every 5 seconds during the run at 1360 m through the stratocumulus layer. This diagram has been annotated in a similar way to Fig. 13(d). It can be seen that through much of the stratocumulus, the main spectral peak is at about 12.5 μm diameter, with a strong minimum in the spectrum at around 6.5 μm. All of the spectra show high concentrations at small droplet sizes, which suggests that the spectra may be bimodal, with another peak at a size smaller than 3.5 μm diameter and hence out of range of the FSSP. In the region of stratocumulus where active cumuli were sampled during the run below cloud, the spectral peak is broad and extends
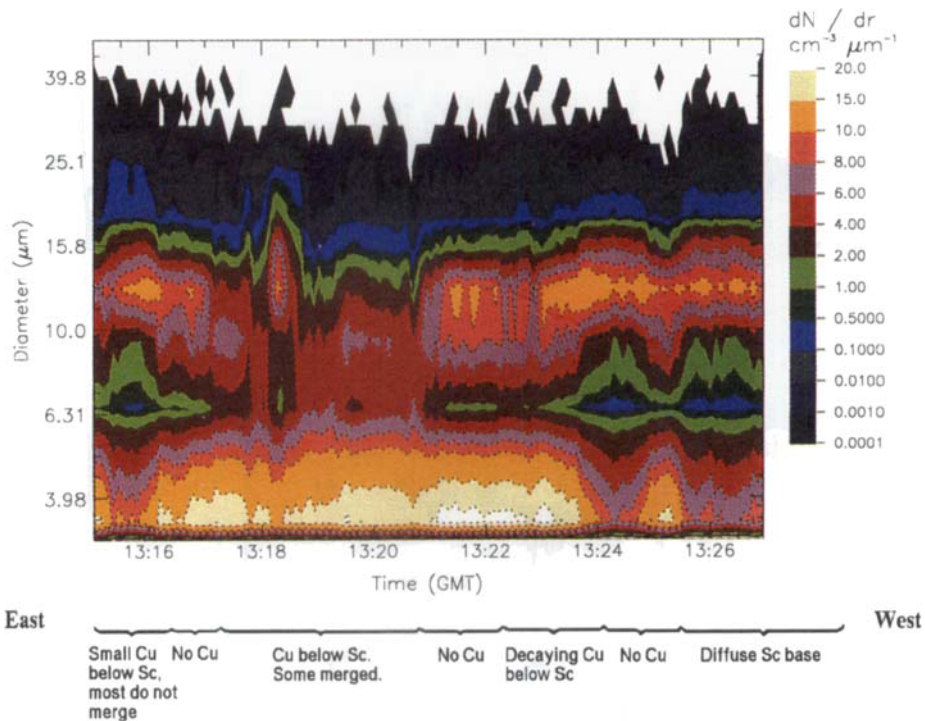
Figure 15. Contoured droplet spectra measured by the FSSP during the horizontal run through the stratocumulus at 1360 m on 18 May 1990, averaged over 5-second intervals.

to larger sizes than in the surrounding regions. This corresponds to the sharp increase in effective radius seen in Fig. 14(b).

Figure 16(a) shows a time-series of the concentration of drops larger than 100 μm diameter, measured using the 2DC probe during the run through cloud at 1360 m and averaged over a minimum of 5 seconds. The variations in the concentration of drizzle-sized drops do not show a clear correlation with the occurrence of cumulus clouds below the stratocumulus, although there is some indication that the lowest concentrations are associated with regions where no cumulus clouds penetrated the stratocumulus. Figures 16(b), (c) and (d) show the total cloud LWC, droplet concentration and effective radius, for droplets in the size range 2.0–800.0 μm diameter, obtained by combining measurements made by the FSSP and 2DC. These time-series are very similar to those in Figs. 13(d) and 14, both in terms of the variations and the absolute values, which suggests that the contribution of the drizzle drops to the total droplet spectrum was small.

(iv) *Radiative effects.* National Oceanic and Atmospheric Administration (NOAA) Advanced Very High Resolution Radiometer (AVHRR) images at 10.8 μm (infrared) and 0.7–1.1 μm (near-infrared) have been used to calculate cloud reflectance and brightness temperatures over the British Isles and the North Sea, at 1313 GMT on 18 May 1990. These are shown in Fig. 17. A stratocumulus sheet is seen to extend over much of the North Sea and the eastern UK, with few variations in cloud-top temperature (Fig. 17(a)). However, the near-infrared image in Fig. 17(b) shows that there are substantial variations in reflectance across the cloud sheet at this time. There are many localized regions of high reflectance over the sea, and comparison with Fig. 17(a) shows that many of these occur in regions of
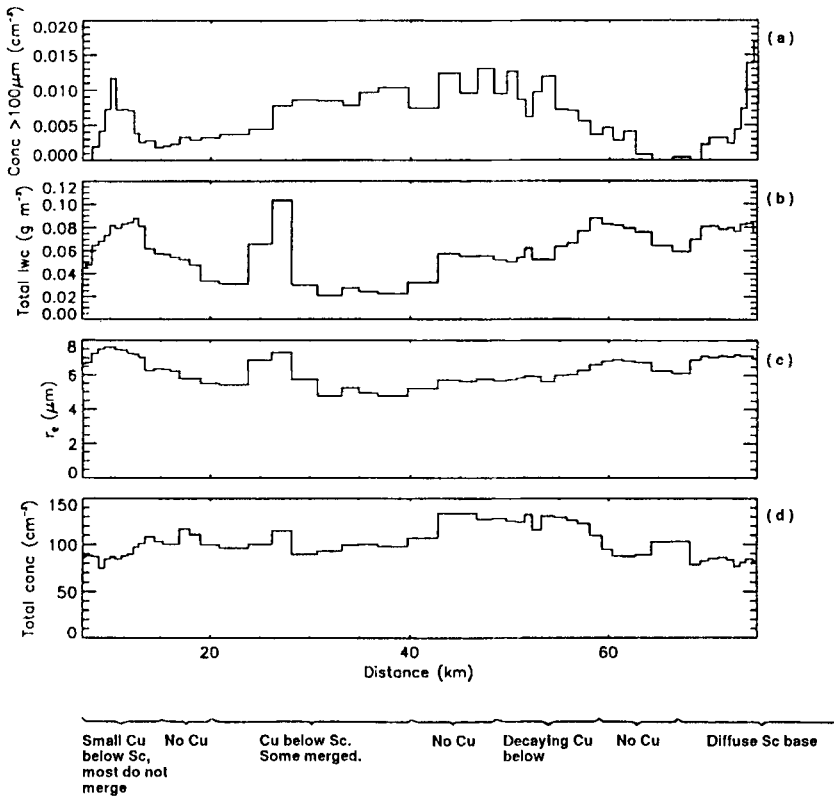
Figure 16.   Measurements made during the run at 1360 m shown in Fig. 15: (a) concentration of drops larger than 100 μm diameter; (b) total liquid-water content of droplets in the size range 2.0–800.0 μm diameter; (c) total droplet-effective-radius; (d) total droplet concentration.

unbroken cloud. This indicates that they are the result of either microphysical variations within the cloud or variations in cloud thickness (and hence liquid-water path), or both.

In order to try to isolate the effects of changing droplet size, radiances at 3.7 μm from the AVHRR data have been analysed. When the thermal component is removed from this signal (assuming that the cloud emissivity is a constant value of 0.85 across the whole scene*), the resulting radiance is a good indicator of droplet size. At this wavelength, there is strong liquid-water absorption, so provided the liquid-water path is not too small, the droplets at cloud top contribute most to changes in the observed radiance. Figure 18 shows radiances at 3.7 μm for the satellite overpass in Fig. 17. In this image, lower radiances (darker areas) represent larger droplet-size. Comparison of Fig. 18 with Fig. 17(b) reveals that the largest droplet-effective-radii within the stratocumulus cloud over the sea correspond to areas of increased reflectance. This implies that there must also be an increase in liquid-water path in these regions, and that this must be either comparable with or greater than the increase in droplet-effective-radius.

Increases in both droplet-effective-radius and cloud LWC were observed within regions of penetrating cumuli in the aircraft measurements in the stratocumulus over the sea. It is, therefore, likely that many of the areas of increased reflectance seen in Fig. 17(b)

* This is because the cloud emissivity is itself a function of cloud-droplet size. In order to retrieve the droplet size from 3.7 μm radiances accurately, an iterative procedure is required, as described by Han et al. (1994).

Figure 17.   (a) Cloud brightness-temperature derived from a NOAA AVHRR image at 10.8 μm (infrared), taken at 1313 GMT on 18 May 1990. (b) Cloud reflectance derived from a NOAA AVHRR image at 0.7–1.1 μm (near-infrared), taken at 1313 GMT on 18 May 1990.
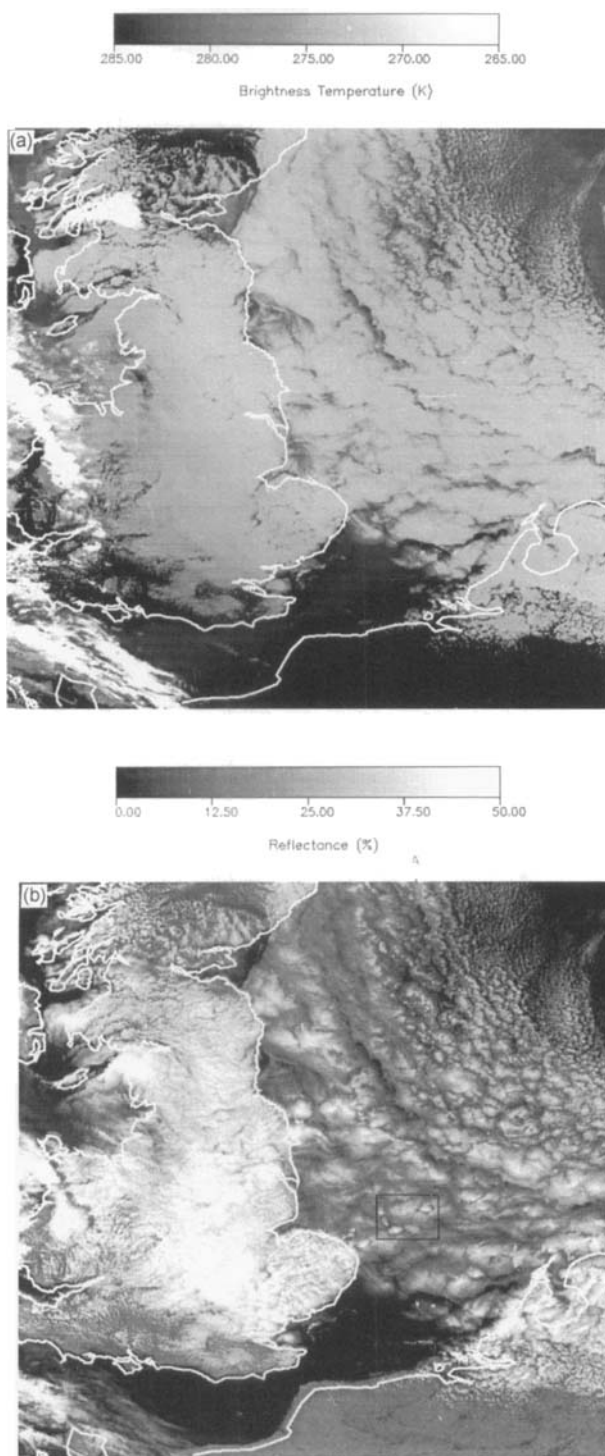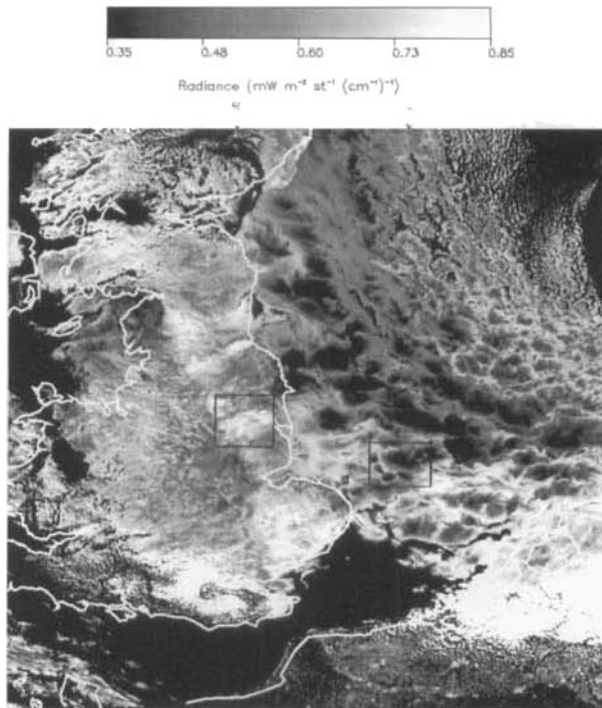
Figure 18.   NOAA AVHRR radiances at 3.7 μm, with the thermal component removed so that the values indicate changes in the droplet effective radius. Darker regions (lower radiance) imply larger droplet-sizes.

are regions of cumulus penetration. The spatial resolution of the AVHRR is ~ 1 km^2, so we would not expect the effects of individual cumulus clouds on the stratocumulus to be necessarily resolved in the satellite images. However, the cumulus clouds were observed to occur in clusters 10–20 km wide, and the clusters increased in size over time. Additionally, within the stratocumulus itself, mixing would be expected to spread the effect of the cumulus clouds laterally. Therefore, regions of increased reflectance on a variety of scales might be expected, with the highest reflectance representing the area of active cumulus clouds within each region. Figure 19(a) and (b) shows enlargements of the regions marked A on Figs. 17(b) and 18 respectively. These images have been enhanced by contrast stretching in order to highlight the main features. The increase in reflectance towards the centres of the areas of active cumulus cloud penetration is well-marked in Fig. 19(a), and is seen to coincide approximately with increases in droplet size seen in Fig. 19(b).

Other details of changes in the cloud microphysics are evident in these images. Marked decreases in droplet size in the form of 'plumes' can be seen along the east coast of England in Fig. 18. These emanate from point sources in several locations, which are known to correspond to pollution sources such as oil refineries and power stations. The effects of such local sources are likely to be similar to the ship-track phenomenon, where the droplet size in stratocumulus is reduced locally due to the introduction of particles from ship plumes (Coakley *et al.* 1987; Radke *et al.* 1989). However, in a decoupled boundary-layer, transport of the aerosol particles emitted from surface sources such as ships or power stations may be inhibited. This was one of the hypotheses to be tested during the Monterey Area Ship Track (MAST) experiment in June 1994. Observations made at midday at many stations around the UK indicate that, at virtually all locations, cumulus clouds were observed below the stratocumulus layer. It is possible that the cumulus clouds helped to
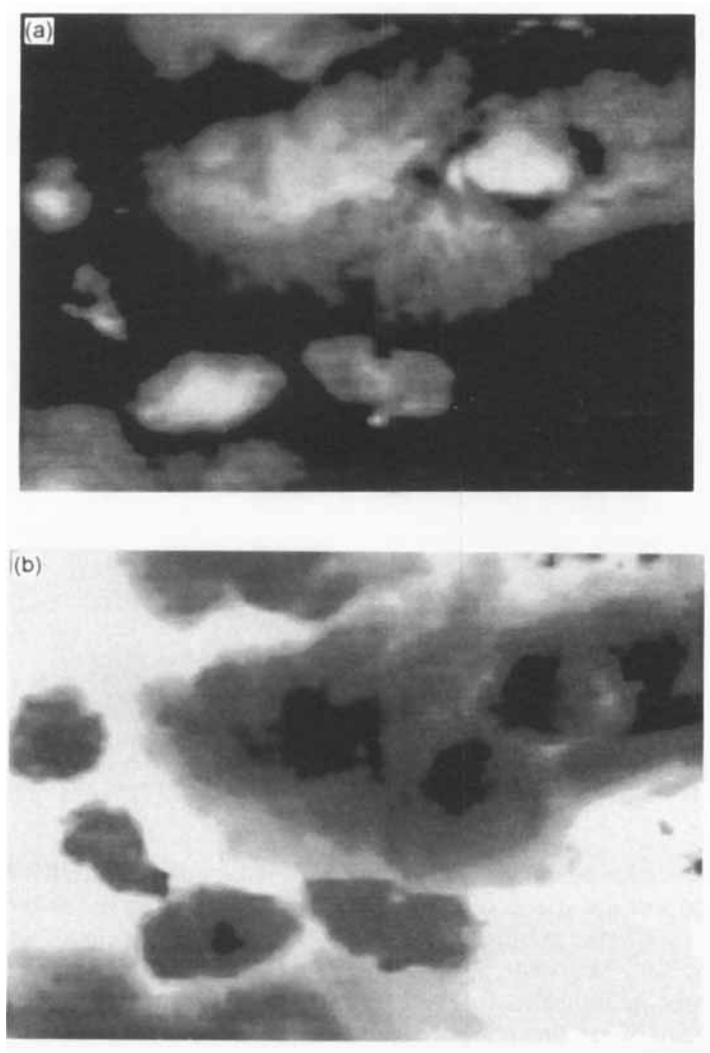
Figure 19.   Enlargements of the region marked A on (a) Fig. 17(b), and (b) Fig. 18. The images have both been
contrast-enhanced in order to highlight the variations in radiance across the region.

enhance transport of the aerosol particles into the overlying cloud layer. The existence of
bright spots within the plumes in the 3.7 μm image (region B on Fig. 18) suggests that
cumulus clouds may be forming within these plumes, and that the droplet size is reduced
locally as more aerosol is brought into the cloud layer. This will be discussed further in a
later paper.

The images in Figs. 17 to 19 illustrate that the penetration of cumulus clouds into
a stratocumulus layer may have a significant effect on the cloud microphysics and hence
radiative properties of the cloud. They also indicate that the cloud properties may be very
sensitive to the type and concentration of aerosol in the boundary layer. The analysis above
highlights the importance of using different wavelength satellite observations for image
interpretation.

4. COMPARISON OF CASE STUDIES IN CLEAN AND POLLUTED AIRMASSES

The case studies described in section 3 highlight the effects of airmass type on the interaction between cumulus and stratocumulus clouds in a decoupled marine boundary-layer. There are many similarities among the three cases:

(a) Localized increases in the values of θ_e and q_T were observed when the cumulus clouds penetrated the cloud layer, indicating that the cumulus clouds were associated with upward transport of air from the SML into the cloud layer, and therefore helped to recouple the cloud layer to the surface.

(b) The intrusion of cumulus clouds was associated with localized increases in LWC in the stratocumulus cloud layer.

(c) The penetrating cumulus clouds increased the geometrical thickness of the cloud layer locally. It is possible that the supply of moisture resulting from the local re-coupling of the cloud layer to the surface was maintaining the stratocumulus.

(d) The cumulus clouds below the stratocumulus tended to form in clusters of the order of tens of kilometres in diameter. This resulted in spatial variations of the same order in the stratocumulus geometrical thickness and microphysical characteristics. Clustering of cumulus clouds on a variety of spatial scales, without the presence of an overlying stratocumulus layer, has often been observed (e.g. Plank 1969; Sengupta *et al.* 1990; Zhu *et al.* 1992). There may be several methods by which cumulus convection may be organized in this way, including mesoscale variations, and the interaction between gravity waves and the convective boundary-layer eddies. Additionally, it has been suggested by several authors (see Sengupta *et al.* 1990), using observations of several different types and sizes of cumulus clouds (including trade-wind cumuli, which form in a similar environment to those in this study), that the cumulus clouds themselves modify their near environments to produce conditions which are favourable for the development of further cumulus clouds. In a decoupled boundary-layer, it is possible that the top of the SML could be raised to a level which is closer to the lifting condensation level of this layer through horizontal convergence associated with a large updraught. Successive cumulus clouds would then tend to form preferentially in this region, whilst on either side of the cluster, the SML depth may be reduced in order to conserve mass. It is not possible to assess the lateral and temporal variations in the depth of the SML accurately enough using the aircraft observations to test this hypothesis.

(e) Increases in cloud optical depth were observed in regions of cumulus cloud penetration from satellite measurements. This implies that although each cumulus cloud may itself be only of the order of a kilometre in diameter, the overall effects of several cumulus penetrations on the radiative properties of a stratocumulus layer are large enough to be observed from space.

The cases differed significantly in the effects of the cumulus clouds on the droplet concentration and average size in the stratocumulus. In the maritime-airmass case (A005), the droplet size increased locally when the cumulus clouds penetrated the stratocumulus, and a small increase in droplet concentration was observed. In the FIRE case (H812), little change in the droplet size was seen in the regions of cumulus cloud penetration, although an increase in droplet concentration was observed. In the Lagrangian case (section 3(a) and Martin *et al.* 1995), which took place in a highly-polluted continental airmass, there was a large increase in droplet concentration associated with the penetrating cumulus clouds. In the early morning of 19 June, when the stratocumulus layer was relatively thick, there was a corresponding decrease in the droplet-effective-radius due to a reduction in

TABLE 1.   SUMMARY OF CLOUD AND AIRMASS CHARACTERISTICS FOR EACH CASE STUDY

Flight	Aerosol concentration SML (cm^{-3})	SL (cm^{-3})	Max. cumulus updraught $(m\ s^{-1})$	Max. drop concentration in penetrating cumulus (cm^{-3})	Max. stratocumulus drop concentration (cm^{-3})	Cumulus thickness (m)	Max. stratocumulus thickness (m)
A213	1950	1100	3.5	500	270	1350	> 700
F3	(1350)	(900)	2.5	225	225	1120	< 120
H812	200–400	200–400	1.2	170	75	550	350
A005	180	180	0.75	140	variable; 80–140	850	300

the proportion of larger (28–48 μm diameter) cloud-droplets in the spectrum. However, on the following day, when the stratocumulus layer was much thinner, the droplets in a cumulus cloud which penetrated the cloud layer were considerably larger than those in the surrounding stratocumulus, and the concentrations were comparable at the stratocumulus level. These observations imply that the nature of the interaction between cumulus clouds forming in a decoupled marine boundary-layer and rising up into a stratocumulus layer may be influenced by the type of airmass in which the clouds form, but that the change in droplet size is also influenced by the relative depth of the cumulus and stratocumulus clouds.

Table 1 shows the boundary-layer characteristics in each of the cases (note that in determining the cumulus cloud thickness, it has been assumed that those cumuli which penetrate the stratocumulus reach the temperature inversion but do not overshoot it; the maximum stratocumulus thickness refers to the thickness of the stratocumulus layer in regions of penetrating cumulus clouds). The Lagrangian case from section 3(a) (and Martin et al. 1995) has been split into two parts, in order to take account of the change in thickness of the stratocumulus and the changes in aerosol concentration which occurred over the 34-hr period. A213 refers to the observations made early on 19 June 1992 in the thicker stratocumulus layer, whilst F3 refers to the thinner cloud layer observed by the NCAR Electra at midday on 20 June (note that the aerosol concentrations given for F3 are those measured with the PCASP on the MRF C-130 on the early morning of 20 June (and are therefore shown in parentheses), since no comparable measurements were made by the NCAR Electra during its flight at midday on 20 June).

It is apparent that the thickness of the cumulus clouds relative to the stratocumulus was greatest for F3 and least for H812. As mentioned above, the droplet size in the penetrating cumulus clouds observed in F3 greatly exceeded that in the surrounding stratocumulus, whereas in H812, little change in droplet size was seen. The thickness of the cumulus clouds relative to the stratocumulus in A213 also exceeded that in H812, but the droplet-effective-radius in the regions of cumulus penetration in A213 was reduced relative to that in the surrounding stratocumulus, which differs from the observations in F3 and H812. The aerosol concentration in the SML in both A213 and F3 was considerably larger than that in the sub-cloud layer, and the vertical velocities associated with the cumulus clouds were relatively high in these two cases. It is likely that both of these factors contributed to the large cumulus cloud droplet concentrations compared with those in the surrounding stratocumulus in A213. In this case, the stratocumulus was much thicker but the cumulus cloud depth was only slightly smaller than in F3, and it appears that the reduction in maximum droplet-size in the cumulus clouds relative to that in the stratocumulus, resulting from the larger droplet-concentration, outweighed the effects of the difference in cloud thickness between the two cloud types. In F3, the effects of entrainment of unsaturated air

over a large fraction of the cumulus cloud depth (as a result of the thinner stratocumulus layer) reduced the droplet concentration to values similar to those in the surrounding stratocumulus. This reduction in droplet concentration, coupled with the large vertical extent of the cumulus compared with that of the stratocumulus, resulted in a significant increase in droplet-effective-radius in the penetrating cumulus cloud. In A005, the airmass was relatively clean and the cumulus cloud depth relative to the stratocumulus thickness was greater than in H812 and A213. Both of these characteristics combined in A005 such that the droplet-effective-radius was increased when the cumulus clouds penetrated the stratocumulus.

The changes in cloud-droplet size within regions of cumulus–stratocumulus interaction in the different cases appeared to influence the growth of drizzle-sized drops in the stratocumulus. In the Lagrangian and FIRE cases, where penetrating cumulus clouds were associated with increases in droplet concentration and decreases in droplet-effective-radius, the concentration of drizzle-sized drops was seen to decrease locally within the regions of cumulus penetration (see Martin et al. (1995) for the Lagrangian case). However, there was no clear correlation between variations in the concentration of drizzle drops and the occurrence of cumulus clouds below the stratocumulus in the maritime-airmass case, where little change in droplet concentration but a large increase in droplet effective radius was observed in the penetrating cumuli. This suggests that the interaction between cumulus and stratocumulus clouds may, in some cases, result in local suppression of drizzle in the stratocumulus layer, but that the extent to which this occurs will depend on the level of pollution in the airmass in which the clouds form. Martin et al. (1995) speculated that the development of large drops in the stratocumulus could actually be aided by the local thickening of the cloud layer which is generally observed in regions of cumulus penetration, and by the introduction, by the cumulus clouds, of droplets which are of a different size from those already existing in the stratocumulus and which may thus provide the differential fall velocities necessary for coalescence. The latter would depend on both the actual and relative sizes of the droplets introduced into the stratocumulus via the cumulus clouds and those already existing in the stratocumulus. The overall effects of cumulus–stratocumulus interaction on drizzle in the stratocumulus are, therefore, difficult to ascertain from these observational studies.

It should also be noted that the changes in microphysics observed in stratocumulus which is affected by cumulus penetration may vary with the distance above the stratocumulus cloud base at which the observation is made. It is possible that in the polluted-airmass case (A213) the droplet-effective-radius in the regions of cumulus penetration may have been similar to that in the surrounding stratocumulus at cloud top, even though a decrease in droplet-effective-radius in the penetrating cumulus was observed at the level within the cloud at which the aircraft was flying. However, it is clear from the preceding discussion that the overall effects of cumulus cloud penetration on the microphysics of a stratocumulus layer may depend on the specific combination of relative cloud thickness, actual and relative cloud-droplet concentrations, and cumulus updraught velocity.

Another important difference between the three cases described in these sections is that they were from different regions of the world, so that the boundary-layer depths, total water contents and the sea-surface temperatures (SSTs) all varied significantly between the cases, as shown in Table 2. The turbulence structure of the boundary layer also differed between the three cases. The fluxes in the Lagrangian case were at least an order of magnitude greater than those in the other two cases, those in H812 being the smallest of the three. The wind speeds, although generally small, also varied between the three cases, with the strongest boundary-layer winds (>8 m s^{-1}) in the Lagrangian case and the lightest winds (<2 m s^{-1}) in H812. A significant wind shear was also seen in the

TABLE 2. SUMMARY OF BOUNDARY-LAYER CHARACTERISTICS FOR EACH CASE STUDY

	Boundary-layer depth (m)	q_T (g kg^{-1})	SST (°C)	Average BL windspeed (m s^{-1})	Wind shear?
A213 and F3	~ 2000	8–9 in SML ~ 5 in sub-cloud layer	18.0–20.5	6–10	yes
H812	770	8.6–9.6	15.5	< 2	no
A005	1400	4–5	11	< 5	no

sub-cloud layer in the Lagrangian case, which may have contributed to the fluxes at this level. These differences show that cumulus–stratocumulus interaction can take place in different regions with widely varying boundary-layer characteristics.

5. SUMMARY

The existence of cumulus clouds rising into stratocumulus has been observed in a number of different regions of the world. The results described in this paper indicate that this situation may result in large lateral variations in the cloud LWC, which may be associated with either a change in the droplet concentration, or the droplet effective radius, or both. Different effects of the penetrating clouds on the stratocumulus microphysics were seen in three cases which took place in different regions of the world and in different airmass types. The change in the cloud microphysics associated with penetrating cumulus clouds appears to be related to the level of pollution within the airmass in which the stratocumulus and cumulus clouds exist. However, there are also other contributing factors, such as the actual and relative cloud thicknesses of the two cloud types. These will be influenced by the boundary-layer depth, the thermodynamic properties of the boundary-layer air and those of the free tropospheric air, the surface fluxes of heat and moisture, and the amount of TKE generated at the cloud top. The latter will determine the height of the stable layer formed when the cloud becomes decoupled from the surface, and will be influenced by the cloud-top temperature, the cloud radiative properties and the incoming solar radiation. The occurrence of wind shear may also affect vertical mixing in the boundary layer. If the cloud layer is drizzling, evaporation of drizzle below the cloud base may also contribute to the decoupling. The thermodynamic characteristics of the boundary-layer air will influence the LWC in both the cumulus and the stratocumulus. Since many of these aspects differed between the three cases studied, it is difficult to attribute the differences between the observed effects of the cumulus–stratocumulus interaction in the three cases to any one cause. This is something which can only be tackled properly using a detailed numerical model with explicit cloud microphysics. However, the observational results imply that there are likely to be significant regional variations in the nature of the cumulus–stratocumulus interaction.

Changes in the microphysics of the stratocumulus will ultimately affect the cloud radiative properties. If, on a global scale, the occurrence of cumulus–stratocumulus interaction is sufficiently widespread, it could have important implications for the earth's radiation budget. Increases in droplet size may decrease the cloud optical depth and thus the reflectance, but when such changes are accompanied by increases in the cloud liquid-water path, which tends to increase the cloud optical depth, the overall effects on the cloud radiative properties are not obvious, and will depend on the fractional change in each parameter. Thus, the cumulus–stratocumulus interaction requires further study in different

regions of the world and in different airmass types, in order that these effects may be quantified.

ACKNOWLEDGEMENTS

REFERENCES

Albrecht, B. A.   1989   Aerosols, cloud microphysics and fractional cloudiness. *Science*, **245**, 1227–1230

Albrecht, B. A., Penc, R. S. and 1985   An observational study of cloud-topped mixed layers. *J. Atmos.*
Schubert, W. H.   *Sci.*, **42**, 800–822

Albrecht, B. A., Randall, D. A. and 1988   Observations of marine stratocumulus during FIRE. *Bull. Amer.*
Nicholls, S.   *Meteorol. Soc.*, **69**, 618–626

Albrecht, B. A., Bretherton, C. S., 1995   The Atlantic Stratocumulus Transition Experiment–ASTEX. *Bull.*
Johnson, D. W.,   *Amer. Meteorol. Soc.*, **76**, 889–904
Schubert, W. H. and
Frisch, A. S.

Baumgardner, D.   1983   An analysis and comparison of five water-droplet measuring in-
                                        struments. *J. Appl. Meteorol.*, **22**, 891–910
                                 1989   Airborne measurements for cloud microphysics. *NCAR Research
                                        Aviation Facility Bulletin No. 24*, NCAR, P.O. Box 3000,
                                        Boulder, CO, USA

Baumgardner, D. and Spowart, M. 1990   Evaluation of the Forward Scattering Spectrometer Probe. Part III:
                                        Time response and laser inhomogeneity limitations. *J. Atmos.
                                        Oceanic Technol.*, **7**, 666–680

Bougeault, P.   1985   The diurnal cycle of the marine stratocumulus layer. A higher-order
                                        model study. *J. Atmos. Sci.*, **42**, 2826–2843

Bretherton, C. S.   1992   'A conceptual model of the stratocumulus–trade–cumulus transi-
                                        tion in the subtropical oceans'. Pp. 374–377 in Proceedings
                                        of the 11th International Conference on Clouds and Precipi-
                                        tation, Montreal, Canada

Coakley, J. A., Bernstein, R. L. and 1987   Effect of ship-track effluents on cloud reflectivity. *Science*, **237**,
Durkee, P. A.   1020–1022

Cooper, W. A.   1988   Effects of coincidence on measurements with a Forward Scattering
                                        Spectrometer Probe. *J. Atmos. Oceanic Technol.*, **5**, 823–832

Edwards, J. M. and Slingo, A.   1996   Studies with a flexible new radiation code. I: Choosing a config-
                                        uration for a large scale model. *Q. J. R. Meteorol. Soc.*, **122**,
                                        689–719

Fouquart, Y., Buriez, J. C.,   1990   The influence of clouds on radiation: a climate modelling perspec-
Herman, M. and Kandel, R. S.   tive. *Rev. Geophys.*, **28**, 145–166

Han, Q., Rossow, W. B. and   1994   Near-global survey of effective droplet radii in liquid water clouds
Lacis, A. A.   using ISCCP data. *J. Clim.*, **7**, 465–497

Hanson, H. P.   1991   Cloud albedo control by cloud-top entrainment. *Tellus*, **43A**, 37–
                                        48

Hudson, J. G. and Frisbie, P. R. 1991   Cloud condensation nuclei near marine stratus. *J. Geophys. Res.*,
                                        96, 20, 795–20, 809

James, D. G.   1959   Observations from aircraft of temperatures and humidities near
                                        stratocumulus clouds. *Q. J. R. Meteorol. Soc.*, **85**, 120–130

Jonas, P. R.   1996   Turbulence and cloud microphysics. *Atmos. Res.*, **40**, 283-306

Kloesel, K. A., Albrecht, B. A. and   1988   'FIRE marine stratocumulus observations—summary of opera-
    Wylie, D. P.   tions and synoptic conditions'. FIRE Technical Report No.
                                                    1, Pennsylvania State University, Dept. of Meteorology, Uni-
                                                    versity Park, PA 16802

Martin, G. M., Johnson, D. W. and   1994   The measurement and parametrization of effective radius in warm
    Spice, A.   stratocumulus clouds. *J. Atmos. Sci.*, **51**, 1823–1842

Martin, G. M., Johnson, D. W.,   1995   Observations of the interaction between cumulus clouds and warm
    Rogers, D. P., Jonas, P. R.,   stratocumulus clouds in the marine boundary-layer during
    Minnis, P. and Hegg, D. A.   ASTEX. *J. Atmos. Sci.*, **52**, 2902–2922

Miller, M. A. and Albrecht, B. A.   1995   Surface-based remote sensing of mesoscale cloud structure during
                                                    ASTEX. *J. Atmos. Sci.*, **52**, 2809–2826

Moss, S. J. and Johnson, D. W.   1994   Aircraft measurements to validate and improve numerical model
                                                    parametrisations of ice to water ratios in clouds. *Atmos. Res.*,
                                                    34, 1–25

Nicholls, S.   1984   The dynamics of stratocumulus: aircraft observations and compar-
                                                    isons with a mixed layer model. *Q. J. R. Meteorol. Soc.*, **110**,
                                                    783–820

Nicholls, S. and Leighton, J. R.   1986   An observational study of the structure of stratiform cloud sheets:
                                                    Part I: Structure. *Q. J. R. Meteorol. Soc.*, **112**, 431–460

Paluch, I. R. and Lenschow, D. H.   1991   Stratiform cloud formation in the marine boundary-layer. *J. Atmos.
                                                    Sci.*, **48**, 2141–2158

Plank, V. G.   1969   The size distribution of cumulus clouds in representative Florida
                                                    populations. *J. Appl. Meteorol.*, **8**, 46–67

Radke, L. ZF., Coakley Jr., J. A. and 1989   Direct and remote sensing observations of the effects of ships on
    King, M. D.   clouds. *Science*, **246**, 1146–1149

Rawlins, F. and Foot, J. S.   1990   Remotely-sensed measurements of stratocumulus properties dur-
                                                    ing FIRE using the C130 aircraft multi-channel radiometer.
                                                    J. Atmos. Sci., **47**, 2488–2503

Rogers, D. P. and Koračin, D.   1992   Radiative transfer and turbulence in the cloud-topped marine
                                                    atmospheric boundary-layer. *J. Atmos. Sci.*, **49**, 1473–1486

Rogers, D. P., Johnson, D. W. and   1995   The stable internal boundary-layer over a coastal sea. Part I. Air-
    Friehe, C. A.   borne measurements of the mean and turbulence structure. *J.
                                                    Atmos. Sci.*, **52**, 667–683

Saxena, V. K. and Kassener Jr., J. L. 1970   'Thermal-diffusion chambers as cloud-nuclei counters'. Pp. 217–
                                                    238 in Proc. U.S. Atomic Energy Commission Symposium on
                                                    Precipitation Scavenging, Washington, NTIS CONF-700601

Sengupta, S. K., Welch, R. M.,   1990   Cumulus cloud field morphology and spatial patterns derived from
    Navar, M. S., Berendes, T. A.   high spatial resolution Landsat imagery. *J. Appl. Meteorol.*,
    and Chen, D. W.   **29**, 1245–1267

Slingo, A.   1990   Sensitivity of the Earth's radiation budget to changes in low clouds.
                                                    Nature, **343**, 49–51

Slingo, A. and Schrecker, H. M.   1982   On the shortwave radiative properties of stratiform water clouds.
                                                    Q. J. R. Meteorol. Soc., **108**, 407–426

Slingo, A., Nicholls, S. and   1982   Aircraft observations of marine stratocumulus during JASIN. *Q.
    Schmetz, J.   J. R. Meteorol. Soc.*, **108**, 833–856

Taylor, J. P.   1992   Sensitivity of remotely sensed effective radius of cloud droplets
                                                    to changes in LOWTRAN version. *J. Atmos. Sci.*, **49**, 2564–
                                                    2569

Turton, J. D. and Nicholls, S.   1987   A study of the diurnal variation of stratocumulus using a multiple
                                                    mixed-layer model. *Q. J. R. Meteorol. Soc.*, **113**, 969–1009

Wang, Q. and Lenschow, D. H.   1995   An observational study of the role of penetrating cumulus in a
                                                    marine stratocumulus-topped boundary-layer. *J. Atmos. Sci.*,
                                                    52, 2778–2787

Zhu, T., Lee, J., Weger, R. C. and   1992   Clustering, randomness and regularity in cloud fields: 2. Cumulus
    Welch, R. M.   cloud fields. *J. Geophys. Res.*, **97**, 20537–20558